Sustainable Food Technology

ROYAL SOCIETY OF CHEMISTRY

PAPER

View Article Online
View Journal

Cite this: DOI: 10.1039/d6fb00067c

Development and application of *Opuntia ficus-indica* mucilage films incorporated with zinc oxide nanoparticles for active packaging of cherry tomatoes

Motlatsi Jane Mohlamonyane,[ab] Jerry Oluwasegun Adeyemi [ab] and Olaniyi Amos Fawole*[ab]

The persistent challenge of food waste, which threatens global food security, has urged exploration of innovative food packaging solutions. Multifunctional nanocomposites have emerged as sustainable packaging alternatives that exhibit antioxidant and antimicrobial effects. This study investigates the development of *Opuntia ficus-indica* mucilage (OFIM)-based films incorporating cellulose nanofiber (CNF) and zinc oxide nanoparticles (ZnO NPs) at 0.2%, 0.4%, and 0.6% (w/w) for postharvest application. The structural and morphological properties of the films were characterized using transmission electron microscopy (TEM), scanning electron microscopy (SEM), X-ray diffraction (XRD), and Fourier-transform infrared spectroscopy (FT-IR). Incorporation of ZnO NPs significantly altered film appearance and color, enhanced opacity, and improved ultraviolet barrier properties. Film thickness and tensile strength increased with higher nanoparticle content (55.95–119.28 MPa), while water vapor transmission showed only slight changes (1.03×10^{-7} to 1.93×10^{-7} g m m^{-2} h^{-1} Pa). Antioxidant assays revealed that all OFIM/CNF/ZnO films exhibited superior antioxidant activity (51–68%) compared to control films. All formulations displayed comparable or enhanced antimicrobial activity against food-borne pathogens relative to neomycin. OFIM/CNF/ZnO (0.4%) demonstrated the best overall performance and was applied as an edible coating on cherry tomatoes alongside control (uncoated), OFIM, and OFIM/CNF treatments. The composite coating effectively delayed weight loss, respiration rate, pH changes, and ascorbic acid degradation, thereby extending shelf-life and preserving fruit quality. Overall, the findings demonstrate that OFIM-based nanocomposite coatings are sustainable active packaging solutions that enhance food preservation and reduce postharvest losses.

Received 9th March 2026
Accepted 23rd April 2026

DOI: 10.1039/d6fb00067c

rsc.li/susfoodtech

Sustainability spotlight

This study developed *Opuntia ficus-indica* mucilage (OFIM)–based nanocomposite films incorporated with green synthesized ZnO nanoparticles as sustainable active packaging materials. The films were derived from plant-based resources and agro-industrial biomass, offering a biodegradable alternative to conventional petroleum-based packaging. The subsequently developed coatings exhibited antioxidant and antimicrobial activity and effectively preserved the postharvest quality of cherry tomatoes by reducing weight loss, respiration rate, and nutrient degradation during storage. Therefore, OFIM-based nanocomposite films provide a promising sustainable packaging approach that can contribute to reducing postharvest losses and improving food preservation, supporting SDG 2 (Zero Hunger) and SDG 12 (Responsible Consumption and Production).

1 Introduction

As the global population continues to grow, the demand for food correspondingly increases. Consequently, food production and safety have emerged as critical priorities.[1] Food packaging is crucial for ensuring safe transportation and protecting food items from contamination, spoilage, and environmental exposure.[2] It also plays a key role in reducing food waste and preserving nutritional quality. Traditional food packaging materials, primarily produced from petroleum-based plastics, are increasingly implicated as unsustainable packaging solutions due to their carcinogenicity, non-biodegradability, and non-renewable properties.[3] These characteristics contribute to environmental pollution, posing significant threats to human health, wildlife, and ecological balance due to their

[a]Postharvest and Agroprocessing Research Centre, Department of Botany and Plant Biotechnology, University of Johannesburg, P.O. Box 524, Auckland Park, Johannesburg 2006, South Africa. E-mail: olaniyif@uj.ac.za

[b]South African Research Chairs Initiative in Sustainable Preservation and Agroprocessing Research, Faculty of Science, University of Johannesburg, Johannesburg, 2006, South Africa

accumulation in ecosystems.[4,5] Considering these concerns, biopolymer-based materials have emerged as promising alternatives offering benefits such as biocompatibility, gas barrier properties, biodegradability, optical properties, and certain biological properties.[6,7]

Natural biopolymers, including lipids, proteins, and polysaccharides, offer a promising material for the development of non-toxic, biodegradable edible films.[8] Amongst those of polysaccharide origin, *Opuntia ficus-indica* mucilage (OFIM) is a notable example that stands out due to its structural integrity, stability, and moisture retention properties.[9–11] This mucilage exhibits exceptional multifunctional properties as an alternative to polysaccharides such as pectin, starch, and alginate. *Opuntia ficus-indica* mucilage (OFIM) is widely known for its natural thickening ability, high water-holding capacity, biocompatibility and exceptional film-forming abilities, attributed to its complex heteropolysaccharide nature.[12] It is recognized as a high-molecular-weight heteropolysaccharide primarily composed of sugars such as xylose, galactose, glucose, rhamnose, arabinose, and galacturonic acid, as well as proteins and uronic acids (particularly glucuronic acid). This chemical composition contributes to its functional properties, including water-binding capacity, rheological behaviour, and emulsifying ability, which are often comparable to those of commercial hydrocolloids such as pectin. Compared to regular polysaccharides like starch and alginate, which often require chemical modification or mixing to work well, OFIM naturally exhibits multifunctional properties due to its complex mix of sugars.[13] Also, unlike many typical polysaccharides, which mainly provide structure, OFIM contains natural bioactive compounds, such as phenolics, that confer antioxidant properties to active packaging systems.[14] Moreover, since it comes from widely available agricultural waste, it is more sustainable and cost-effective, making it a strong candidate for new biodegradable packaging materials.[15] The high molecular weight of this mucilage contributes to its excellent thickening ability and high viscosity, making it a promising biopolymer for food packaging applications.[16,17] This material has been reported to possess film-forming and coating properties, highlighting its effectiveness as a sustainable packaging material.[18] However, due to its hydrophilic nature, it exhibits limited mechanical, barrier, and decay resistance properties, which constrain its application in food packaging.[19] As result, the development of effective composite edible films using OFIM necessitates the incorporation of supplementary materials such as cellulose nanofibers (CNFs) and the functionalization using active biological ingredients.[20]

The incorporation of natural fillers including CNFs has been well documented in the literature to enhance the resulting physicochemical properties.[19,21–23] As such, CNFs have gained recognition due to their excellent mechanical strength, versatility, and biodegradability.[24] These nanofillers facilitate the formation of a strong network within the film base matrix, thereby enhancing the film's hydrophobicity, mechanical durability, and structural integrity, which are essential for maintaining quality and preserving the freshness of packaged food products.[22,25–27] Concurrently, green-synthesized ZnO NPs mediated using plant extracts have gained attention as effective antimicrobial and antioxidant additives for food-contact films and coatings.[28–30] This green synthesis approach employs plant-derived phytochemicals such as terpenoids, carbohydrates, proteins, alkaloids, saponins, and flavonoids as natural reducing and stabilising agents, providing a sustainable and less toxic alternative to conventional chemical synthesis methods.[31] Compared to conventionally made or commercially available ZnO nanoparticles, green-synthesized ZnO often has phytochemical residues on its surface. These residues enhance dispersion stability and compatibility with biopolymer matrices, which may, in turn, enhance antimicrobial and antioxidant properties, thereby improving overall performance. Thus, ZnO NPs have been extensively used in various industries due to their unique properties, including photocatalytic activity, anti-corrosion effects, low electron conductivity, excellent heat resistance, antioxidant effects, and antibacterial properties.[32] Additionally, they are classified as 'Generally Recognized as Safe (GRAS)' by the US Food and Drug Administration (FDA) for both human and animal consumption when in their bulk form.[30] Consequently, ZnO NPs are used as antimicrobial agents in active food packaging systems to inhibit foodborne pathogens, mitigate contamination and spoilage, and prevent postharvest losses by enhancing food quality and safety.[30,33]

Building on our previous finding, in which ZnO NPs synthesized from OFI cladode peel wastes exhibited superior biological properties compared to those synthesized from OFIM residue wastes,[31] the present study developed OFIM-based films infused with CNF and varying concentrations of ZnO NPs synthesized exclusively from OFI cladode peel waste. The physicochemical, antimicrobial, and antioxidant properties of the resulting nanocomposite films were evaluated for their suitability as an active packaging material for food preservation. Finally, the best-performing formulation was applied as an edible coating to cherry tomatoes to assess its effectiveness in retaining postharvest quality.

2 Materials and methods

Cellulose nanofibers (CNFs) (Valida S231C) were obtained from Sappi South Africa as a fibrillated cellulose aqueous suspension made from wood pulp. The material consists of about 8 ± 0.5 wt% cellulose and 92 ± 0.5 wt% water, with a high degree of fibrillation (≥91% fines). The CNF suspension has a high viscosity (≥520 mPa s at 1 wt% and 100 s^{-1}, 20 °C) and a near-neutral pH (7.0–9.0), indicating its ability to form an interconnected fibrillar network. Before use, the suspension was freeze-dried to produce a dry powder for mixing into the film matrix. This process was carried out to enable controlled dispersion during film preparation. Although the supplier does not provide specific size details, cellulose nanofibers typically have diameters in the nanometer range (≈5–60 nm) and lengths extending into the micrometer range, resulting in high aspect ratios (>100). These characteristics enhance their reinforcing quality in polymer matrices. All other chemicals used in this study were sourced from Sigma-Aldrich (South Africa) and were of analytical grade.

2.1 Preparation of chemicals and materials

The *Opuntia ficus-indica* cladodes (cv Morado) were sourced from Ubali Pomegranate & Prickly Pear Farm located in Pretoria, South Africa (25°38′31.9″ S, 28°27′33.0″ E), and subsequently transported to the Postharvest Research Centre at the University of Johannesburg. Mature cladodes were selected for mucilage extraction. All reagents utilized for this study were procured from Sigma-Aldrich (South Africa) and were used without further purification.

2.2 Extraction of OFI cladode mucilage

Mucilage extraction was performed following established methodologies documented in the literature.[34] Briefly, the cladodes were peeled, resulting in cladode peel waste, and the remaining cladode pulp was diced into cubes and microwaved for 4 min. The softened pulps were then blended and centrifuged at 8000 rpm and 4 °C for 15 min to isolate the OFI mucilage (OFIM). The resulting mucilage was then freeze-dried to obtain a powder, which was stored in a sealed container until further use.

2.3 Biosynthesis of ZnO NPs from OFI cladode peel wastes

As previously detailed in our report,[31] the extraction of cladode peel waste was conducted by dissolving 20 g of powdered waste in 200 mL of distilled water at 70 °C for 2 h. The solution was subsequently filtered using Whatman No. 1 filter paper. Following filtration, approximately 200 mL of the resultant extracts was transferred to a 500 mL beaker, whereupon 100 mL of a 1 mM $Zn(CH_3CO_2)2\cdot 2H_2O$ solution was added. This mixture was then maintained under alkaline conditions. This reaction mixture was heated at 70 °C for 2 h with continuous stirring, resulting in a visible color change to off-white, indicating nanoparticle formation. Following this, the mixture was centrifuged, and the resulting residue was washed with distilled water and 100% methanol to remove unreacted materials. This residue was subsequently oven-dried at 50 °C for 12 h and calcined at 400 °C for 3 h. Crystalline nanoparticles, denoted as ZnO, were obtained and used at various concentrations to formulate OFIM-based films. The biosynthesized ZnO nanoparticles exhibited predominantly spherical morphology with minor agglomeration, as confirmed by SEM and TEM analyses. Particle size distribution analysis revealed a mean particle size of approximately 24.33 nm. FTIR spectra showed characteristic peaks corresponding to hydroxyl (–OH), C–H, C–O, and Zn–O stretching vibrations, indicating the involvement of bioactive phytochemicals, particularly phenolic compounds, in the reduction and stabilization of the nanoparticles. These findings are consistent with our previously reported study. Other detailed physicochemical characterization of the synthesized ZnO, particle size distribution histogram, and SEM/TEM analysis have already been reported in our earlier study.[31]

2.4 Formulation of OFIM-based films (OFIM/CNF/ZnO)

Following the previously reported approach with modifications,[6,8] a 3% solution of the prepared mucilage powder was prepared by dissolving it in 100 mL of distilled water for 1 h under continuous stirring at ambient temperature to ensure complete hydration. Afterward, a mixture of 1 mL of canola oil and Tween 80 was added to the mixture to enhance flexibility. In addition, glycerol (20% v/w relative to OFIM) was introduced into the mixture as a plasticizer and allowed to stir for an extra 15 min. Following these additions, cellulose nanofibers (CNFs) at a concentration of 1% w/w relative to dry OFIM were added, and the mixture was heated for an additional 20 min at 50 °C. Furthermore, various concentrations of biosynthesized ZnO NPs (0, 0.2, 0.4, and 0.6 (w/w %) relative to OFIM) were subsequently incorporated and allowed to mix for 30 min. The resulting film-forming solutions were then homogenized and subjected to ultrasonication for 1 h to minimize air bubble formation. Finally, 30 mL of the film-forming solutions were transferred into Petri dishes and oven-dried at 50 °C for 72 h. The resulting compositions of the fabricated films are summarized in Table S1 in the SI.

2.5 Color attributes

The color attributes of the films, including lightness (L^*), redness/greenness (a^*), and yellowness/blueness (b^*), were evaluated using a colorimeter (Konica Minolta Chroma Meter CR-400, Osaka, Japan). All measurements were performed in triplicate. The total color difference (ΔE) was calculated using the following equation:

$$\Delta E = [(\Delta L)^2 + (\Delta a)^2 + (\Delta b)^2]^{0.5} \quad (1)$$

where ΔL, Δa, and Δb denote variation in each color value compared to the color of control films.[35]

2.6 Moisture content (MC)

Moisture content was determined following the procedure in the literature.[4] In triplicate, dried strips of nanocomposite OFIM-based films were cut into fragments (2 cm × 2 cm). The initial mass of the fragments was determined utilizing a measuring scale (RADWAG Electronic PS 4500, R2.M, Poland, 0.01 accuracy). The fragments were then oven-dried at 100 ± 1 °C for 24 h, after which the final mass was recorded. The MC was calculated using the following equation:

$$\mathrm{MC}(\%) = \frac{M_0 - M_1}{M_0} \times 100 \quad (2)$$

where M_0 and M_1 denote the film's initial mass (g) before and after drying, respectively.

2.7 Water solubility (WS)

Water solubility was determined using the procedure outlined in the literature with some adjustments.[6] In triplicate, the nanocomposite OFIM-based films were cut into fragments (2 cm × 2 cm) and then oven-dried at 50 °C for 24 h. Afterward, the initial mass of the fragments was recorded using a measuring scale (RADWAG Electronic PS 4500, R2.M, Poland, 0.01 accuracy). The fragments were then dipped in distilled water (30 mL) and allowed to stir overnight at 50 °C. After immersing, the non-

solubilized pieces were filtered using Whatman filter paper, then oven-dried at 100 °C for 2 h. The filtered pieces were then oven-dried at 100 °C for 2 h, and their final masses were noted. The WS percentage was determined using the following equation:

$$\mathrm{WS}(\%) = \frac{W_{\mathrm{initial}} - W_{\mathrm{final}}}{W_{\mathrm{initial}}} \times 100 \quad (3)$$

where W_{initial} and W_{final} denote the initial and final mass of the films, respectively.

2.8 Water vapor transmission rate (WVTR)

The water vapor transmission rate (WVTR) properties of nanocomposite OFIM-based films were evaluated using the procedure in the literature with some slight modifications.[6] Dried films were cut into sections (8 cm × 8 cm) in triplicate. About 25 mL of distilled water was transferred into measuring cups, with film sections mounted onto them. Subsequently, parafilm was employed to securely seal the cups, thereby establishing watertight conditions. The initial mass was recorded using a precision scale (RADWAG Electronic PS 4500, R2.M, Poland, with an accuracy of 0.01 g), and the samples were then placed in an oven at 50 °C, maintained at 50% relative humidity. The change in weights of each measuring cup was recorded at hourly intervals for 8 h. Water vapor transmission rate (WVTR) was determined using the following equation:

Weight changes for each cup were measured every hour for 8 h.

$$\mathrm{WVTR} = \frac{\left(\frac{\mathrm{Slop}}{A}\right) \times X}{P(R_1 - R_2)} \quad (4)$$

WVTR (g mm^{-1} hr^{-1}) is represented as slope (g h^{-1}) divided by the total surface area (mm^2). X (mm) denotes the thickness of films, and Δp is described as p (R_2–R_1), where R_1 is 0% and R_2 is 50%.

2.9 Mechanical properties

2.9.1 Tensile strength. The tensile strength of the films was determined using a texture analyzer (GÜSS-FTA, Strand, South Africa). The films were cut into fragments (4 cm × 8 cm), and each fragment was subjected to puncture using an 8 mm probe. The maximum puncture resistance force exhibited by each film section was recorded. The tensile strength was calculated by dividing the puncture resistance force by the cross-sectional area of the film fragments, as delineated in the following equation:

$$\mathrm{TS(MPa)} = \frac{F_{\mathrm{max}}}{L \times W} \quad (5)$$

where F_{max} denotes the maximum puncture resistance force (N), L represents the length (cm), and W denotes the width (cm) of the films.[36]

2.9.2 Thickness. The thickness of the films was measured employing a digital micrometer with an accuracy of ±0.001 mm. Measurements were taken at five distinct points, randomly selected near the center of the film, including the midpoint. Subsequently, mean values of the film thickness were calculated ($n = 5$).[4]

2.10 Light transmittance and opacity

The optical barrier properties of the nanocomposite films were evaluated using a UV spectrophotometer (Spectrum Instruments, SP-UV 300, Shanghai, China) within a wavelength range of 400 to 800 nm. For the analysis, the dried films were cut into fragments, measuring 1 cm × 3 cm, and placed perpendicularly in a plastic cuvette to measure light transmittance, using an empty plastic cuvette as a reference. The opacity of the films was recorded by measuring absorbance at 600 nm, which was subsequently divided by the film thickness,[37] as illustrated in the following equation:

$$\mathrm{Opacity} = \frac{A_{600}}{X} \quad (6)$$

where A_{600} denotes the absorbance value recorded at 600 nm and X denotes film thickness.

2.11 X-ray diffraction (XRD)

The crystalline properties of the ZnO-incorporated films were analyzed using an X-ray diffractometer (PANalytical Empyrean, XPERT-PRO, USA) within a 2θ range of 20° to 80°, a scanning speed of 2 min^{-1}, and Cu Kα radiation (λ = 1.5418 Å) at room temperature. For the analysis, circular-shaped films (diameter 3.5 cm) were used, and each film section was positioned on the X-ray exposure stage.[35]

2.12 Scanning electron microscopy

The surface morphology of the films was examined using scanning electron microscopy (Tescan Vega 3, Brno, Czech Republic). Each film fragment was subjected to carbon coating, and images were captured at various magnifications.[38]

2.13 Fourier transform infrared spectroscopy (FT-IR)

An FTIR spectrophotometer (Thermo Scientific Smart iTR, Attenuated Total Reflectance, Thermo Fisher Scientific Inc., USA) was used to analyze the structural interactions among the OFIM powder, CNF, and synthesized ZnO NPs with spectra ranging from 4000 to 400 cm^{-1}.[39]

2.14 Biological properties of the films

2.14.1 DPPH radical scavenging assay. The antioxidant properties of the nanocomposite films were evaluated using a methodology reported in the literature using the DPPH (2,2-diphenyl-1-picrylhydrazyl) assay.[6] Film sections (50 mg) were immersed in 10 mL of distilled water in a centrifuge tube and vigorously mixed for 5 min. The mixture was then centrifuged for 5 min at 5000 rpm at 4 °C. Afterward, 3 mL of supernatant was collected and combined with 1 mL of methanolic DPPH, then incubated in the dark at room temperature for 30 min. Absorbance values were recorded using a UV spectrophotometer (Spectrum Instruments, SP-UV 300) at 517 nm. The percentage of radical scavenging activity was calculated using the following equation:

$$\text{DPPH scavenging activity}(\%) = \frac{\text{Abs}_{\text{DPPH}} - \text{Abs}_{\text{DPPH/sample}}}{\text{Abs}_{\text{DPPH}}} \times 100\% \quad (7)$$

where Abs_{DPPH} represents the absorbance of the methanolic DPPH solution and $\text{Abs}_{\text{DPPH/sample}}$ refers to the absorbance of the methanolic DPPH solution mixed with the film samples.

2.14.2 Ferric reducing antioxidant power (FRAP) assay. The Ferric Reducing Antioxidant Power (FRAP) of the films was evaluated using a procedure reported in the literature with slight adjustments.[40] A fresh FRAP solution was prepared in an Erlenmeyer flask by combining 20 mM ferric chloride and 10 mM 2, 4, 6-tripyridyl-*s*-triazine (TPTZ) in 0.25 M acetate buffer (pH 3.6).[41] Film section samples (50 mg) were immersed in 10 mL of distilled water in a centrifuge tube and vortexed for 5 min, followed by centrifugation at 5000 rpm for an additional 5 min at 4 °C. The resulting supernatant (90 μL) was mixed with distilled water (270 μL), followed by the addition of 2.7 mL of the freshly prepared FRAP reagent solution and incubated for 30 min in the dark at room temperature. Absorbance values were recorded using a UV spectrophotometer (Spectrum Instruments, SP-UV 300) at a wavelength of 593 nm. The results were expressed as Trolox (mM) equivalents per milligram of film fragments (mM TE mg^{-1}).

2.14.3 $ABTS^+$ radical scavenging activity (RSA) assay. The $ABTS^+$ radical scavenging activity of the nanocomposite films was assessed in accordance with the protocol reported in the literature with some changes.[6] A mixture of 2.45 mM potassium persulfate and 7 mM ABTS was prepared in a 1 : 1 stoichiometric ratio and incubated at room temperature for 12 to 16 h in the dark. Following incubation, 1 mL of the resulting mixture was diluted with 100% methanol to achieve an absorbance of 0.704 ± 0.001 at 734 nm. Film fragment samples (50 mg) were immersed in 10 mL of distilled water and vortexed vigorously for 5 min, followed by centrifugation at 5000 rpm for another 5 min at 4 °C. About 3 mL of the resulting supernatant was combined with 1 mL of the methanolic ABTS mixture, and the mixture was incubated for 30 min at room temperature. Absorbance values were measured utilizing a UV spectrophotometer (Spectrum Instruments, SP-UV 300, Shanghai, China) at 734 nm. The percentage of $ABTS^+$ radical scavenging activity was estimated using the following equation:

$$\text{ABTS scavenging activity}(\%) = \frac{\text{Abs}_{\text{ABTS}} - \text{Abs}_{\text{ABTS/samples}}}{\text{Abs}_{\text{ABTS}}} \times 100(\%) \quad (8)$$

where Abs_{ABTS} denotes the absorbance of the methanolic ABTS solution, while $\text{Abs}_{\text{ABTS/samples}}$ refers to the absorbance of the methanolic DPPH solution mixed with the film samples.

2.14.4 Antimicrobial properties. Antimicrobial activity of the films was investigated utilizing the agar well disc diffusion assay against common foodborne pathogens (*Staphylococcus aureus* ATCC 29213, *Listeria monocytogenes* ATCC 7644, *Escherichia coli* ATCC 35218, and *Candida albicans* ATCC 14053. Film samples (8 mm diameter) were placed on the surface of the Mueller–Hinton agar plates and incubated for 24 h at 37 °C. Following incubation, the zones of inhibition were measured to evaluate the antimicrobial properties.[4]

2.15 Release profiling

The release profile of the developed nanocomposite films was assessed using the method described by Priyanka *et al.* (2024),[41] with slight modifications. Film fragments measuring 2 cm × 2 cm were immersed in 10 mL of distilled water and incubated under shaking conditions at 37 °C. At 3 h intervals, 1.5 mL of the sample solution was collected and used to measure the surface plasmon absorption maxima at 370 nm.

2.16 Application on cherry tomatoes

2.16.1 Procurement and handling of tomatoes. Cherry tomatoes were obtained from the Johannesburg Market and subsequently transported to the Postharvest Research Centre at the University of Johannesburg. The fruits were then sorted for uniformity in size, color, and the absence of defects. Following this, they were rinsed with a 0.1% sodium hypochlorite solution to minimize contamination.

2.16.2 Application of edible coating. The fruits were immersed in their respective composite coatings for 3 min. Four distinct treatments were administered: control fruits (dipped in distilled water), OFI mucilage alone, OFI mucilage with cellulose nanofiber (OFIM/CNF), and OFI mucilage with CNF and ZnO (OFIM/CNF/ZnO (0.4%). Following treatment, the fruits were permitted to air dry at room temperature for 1 hour before being packaged in ventilated punnets. Each treatment consisted of three replicates, with five fruits per replicate, as shown in Fig. S1 in the SI. The fruits were stored at ambient temperature (85 ± 2% relative humidity at 25 °C ± 2 °C) for 12 days, and postharvest quality was assessed at 2-days intervals.[42]

2.16.3 Physiological properties

2.16.3.1 Weight loss. The weight loss percentage of the cherry tomatoes was determined using the method reported in the literature.[43] At the beginning of the storage period, five random cherry tomatoes from each replicate were selected and weighed using an electronic weighing scale (RADWAG Electronic PS 4500.R2.M, Poland; accuracy 0.01 g) and recorded as W_i (initial weight). And thereafter, the same fruits were consistently weighed at 2-days intervals, noted as W_f. Weight loss was then determined using the following equation:

$$\text{WL}(\%) = \frac{W_i - W_f}{W_f} \times 100 \quad (9)$$

2.16.3.2 Respiration rate. The respiration rate of the tomatoes was assessed using the closed system approach.[42] Five fruits per replicate were placed in a 400 mL airtight container sealed with a lid fitted with a rubber septum and incubated for 1 h at room temperature. After incubation, the carbon dioxide produced inside the container was measured using an infrared gas analyzer (Checkmate 3, PBI Dansensor, Ringsted, Denmark). Respiration rate was presented as mL CO_2 kg^{-1} h^{-1}.

2.16.3.3 Firmness. The firmness of the fruits was assessed following the method in the literature.[34] A texture analyzer

(Agrosta Texture Analyser, Calib, France) equipped with a 5 mm diameter probe penetrated the fruit at a speed of 1.0 mm s^{-1} to a distance of 10 mm. The obtained data were recorded as the maximum force in Newtons.

2.16.4 Physicochemical attributes

2.16.4.1 Color attributes. The color of the fruits was determined using a calibrated colorimeter (Konica Minolta Chroma Meter CR-400, Osaka, Japan). In triplicate, the following parameters were measured: L^* (lightness/brightness), and a^* (red/green spectrum) values.[44]

2.16.4.2 Total soluble solids and pH. Tomato juice was extracted from each treatment using a Salton juice extractor (Brunswick, Canada). The pH of the juice was measured using a pH meter, and total soluble solids were determined using a digital refractometer (Atago, Tokyo, Japan) and expressed in ° Brix.[42]

2.16.5 Phytochemical analysis

2.16.5.1 Ascorbic acid content. The ascorbic acid (AA) content in the tomato juice was measured following the method in the literature.[45] In brief, 1 mL of fruit juice was combined with 4 mL of 1% metaphosphoric acid and sonicated for 10 min. Then, about 50 μL of the resulting clear supernatant was mixed with 200 μL of 2,6-dichlorophenolindophenol (dye), transferred to a 96-well microplate, and incubated at room temperature for 30 min. After incubation, the absorbance values were measured at 515 nm. L-Ascorbic acid was used as a reference to construct a standard curve for quantifying the ascorbic acid content in each sample. The results were expressed as micrograms of ascorbic acid equivalent per mL of cherry tomato juice (μg AAE mL^{-1}).

2.16.5.2 Total lycopene content. The total lycopene content of the tomato juice was quantified following the method in the literature with some changes.[46] Approximately 1 mL of fruit juice was homogenized with ethanol and hexane (1 : 1) containing 0.02% 2,6-di-*tert*-butyl-4-methylphenol (BHT). The resulting mixture was sonicated for 10 min under the following conditions: frequency of 50 Hz, temperature of 25 °C, and power of 500 W. Subsequently, the absorbance was measured at 470 nm using a UV-Vis spectrophotometer in a dark environment.

2.17 Statistical analysis

One-way analysis of variance (ANOVA) was used to analyze the obtained data for film characterization using STATISTICA software (STATISTICA 14.0, TIBCO, Tulsa, OK, United States), with Duncan's multiple tests to depict the significant difference ($p < 0.05$). Microsoft Excel (Microsoft Corporation v13.0, Washington, DC, USA) was therefore used for graphical presentation. The data collected for postharvest application were analyzed using statistical software (GenStat 20th Edition, VSN International, Hemel Hempstead, UK) using analysis of variance (ANOVA). Duncan's multiple range test was used to separate the mean values using the least significant difference at 5% significant level.

3 Results and discussion

3.1 Color attributes

Color is a crucial parameter in choosing a suitable food packaging material, as it influences both the consumer preference and the product's visual appearance.[47] The color attributes (L^*, a^*, and b^*) and the total color difference (ΔE) of the nanocomposite film are presented in Table 1. Noticeable changes in the color properties of the films were observed, as shown in Fig. 1, upon incorporating ZnO NPs into OFIM-based film matrix. As the concentration of ZnO NPs increased, a slight yet statistically significant increase in L^* (lightness) values ($p < 0.05$) was observed, with the highest L^* value (52.13 ± 0.32) recorded with OFIM/CNF/ZnO (0.6%), compared to the control film (49.27 ± 0.71). This increase in lightness can be attributed to enhanced light reflection, which plays a crucial role in shielding and protecting food products that are susceptible to oxidation or light exposure.[48] Regarding the a^* values (green/red), they remained consistently low across all film formulations; however, a marginal increase was observed in the OFIM/CNF/ZnO (0.4%) film, resulting in an a^* value of 0.93 ± 0.12, indicating a slight shift in coloration relative to the control film. On the other hand, the b^* values (blue/yellow) varied across the formulations, increasing with higher ZnO concentrations, with the OFIM/CNF/ZnO (0.4%) film exhibiting the highest b^* value (8.57 ± 0.20), indicating enhanced yellow coloration. This observation may be due to the inherent off-white hue of ZnO NPs. Overall, a significant variation in total color difference (ΔE) between the OFIM/CNF films and those nanocomposite films was observed, with the OFIM/CNF/ZnO (0.6%) film exhibiting the greatest ΔE (3.00). This value exceeds the perceptibility threshold, indicating visibly detectable changes relative to the control, as shown in Fig. 1. A similar observation was reported

Table 1 Color attributes of OFIM-based films incorporated with cellulose nanofiber and various concentrations of ZnO nanoparticles[a]

Film samples	L^*	a^*	b^*	ΔE
OFIM/CNF	49.27 ± 0.71^{b}	0.60 ± 0.06^{b}	6.80 ± 0.50^{c}	1.04 ± 0.31^{b}
OFIM/CNF/ZnO (0.2%)	50.57 ± 0.43^{ab}	0.30 ± 0.06^{c}	5.43 ± 0.12^{d}	1.99 ± 0.23^{ab}
OFIM/CNF/ZnO (0.4%)	51.47 ± 0.28^{a}	0.93 ± 0.12^{a}	8.57 ± 0.20^{a}	1.85 ± 0.94^{ab}
OFIM/CNF/ZnO (0.6%)	52.13 ± 0.32^{a}	0.67 ± 0.03^{b}	7.63 ± 0.27^{b}	3.00 ± 0.37^{a}

[a] Mean values with their corresponding ± standard deviation ($n = 3$). Numerical values with different superscript letters indicate statistically significant differences within the same column, as determined by Duncan's multiple range test ($p < 0.05$). OFIM: *Opuntia ficus-indica* mucilage; CNF: cellulose nanofiber; ZnO: zinc oxide NPs.

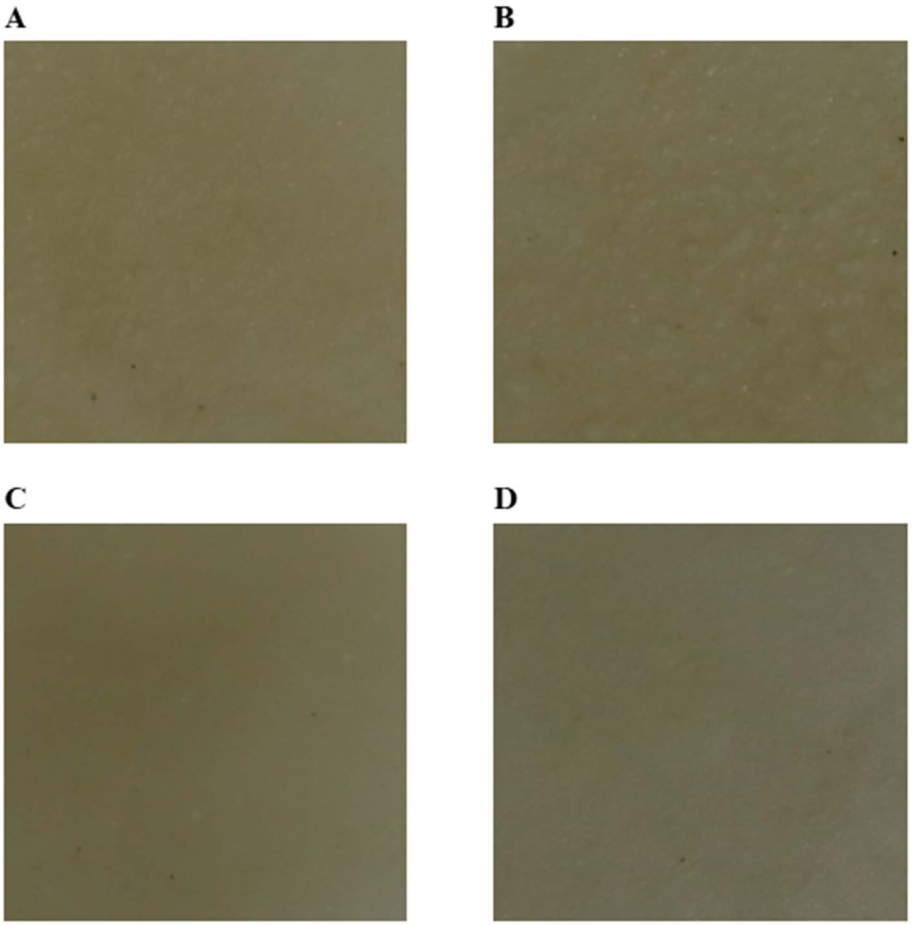

Fig. 1 Visual appearance of OFIM-based films incorporated with different concentrations of ZnO NPs. OFIM: *Opuntia ficus-indica* mucilage; CNF: cellulose nanofiber; ZnO: zinc oxide NPs. Notes: (A) OFIM/CNF, (B) OFIM/CNF/ZnO (0.2%), (C) OFIM/CNF/ZnO (0.4%) and (D) OFIM/CNF/ZnO (0.6%).

in the study conducted by Foghara *et al.*[49] which involved the incorporation of ZnO NPs into a basil seed mucilage biopolymer matrix.

3.2 Moisture content and water solubility

Moisture content (MC) in food packaging materials is important for preserving and maintaining the quality of food products by limiting unwanted moisture transfer, which can result in food spoilage and stimulate microbial growth.[50] A higher MC value (39.70 ± 4.76%) was recorded at OFIM/CNF/ZnO (0.2%) film, which may be attributed to the hydrophilic nature of ZnO NPs at low concentrations, which increases water-binding capacity like the report by Leta *et al.*[6] However, at higher loading, OFIM/CNF/ZnO (0.4% and 0.6%) nanocomposite films returned to the similar level to the control film as observed in Table 2, suggesting that the interaction of the ZnO–polymer created a denser network at higher loading, reducing the water absorption properties. In contrast, no statistical difference was observed in water solubility (WS) across all film formulations ($p > 0.05$), which ranged from 82.32% to 85.41%. The high WS is attributed to the strong moisture affinity of OFIM due to its hydrophilic properties and the significant presence of OH^- groups on the polysaccharide chains. Similar findings were reported by Mkhari *et al.*[8] who found that OFIM with cellulose nanofibers showed the lowest water solubility at 11.52%. In contrast, the films incorporated with encapsulated beetroot powder exhibited significantly higher water solubility, reaching 56.15%, which is attributed to the hydrophilic nature of the mucilage.

3.3 Water vapor transmission rate

The water vapor transmission rate (WVTR) of the films is presented in Table 2. The WVTR of the control film (OFIM/CNF) was 1.03×10^{-7} g mm^{-1} h^{-1}, with no significant change observed upon incorporation of 0.2% and 0.4% ZnO NPs. However, a significant increase was observed at a higher ZnO NP concentration, recorded as 1.93×10^{-7} g mm^{-1} h^{-1}. This trend aligns with other reports in the literature such as those by Petchwattana *et al.*[51] who observed that low nanoparticle concentrations often enhance barrier properties by creating a more tortuous vapor diffusion pathway, and higher loading may have a converse effect. Marra *et al.*[52] attributed such converse increases to the formation of additional free volume at the polymer–nanoparticle interface, facilitating polar water

Table 2 Moisture content, water solubility, and water vapor transmission rate of OFIM-based films incorporated with cellulose nanofiber and various concentrations of ZnO nanoparticles[a]

Film samples	MC (%)	WS (%)	WVTR ($\times 10^{-7}$ g mm^{-1} h^{-1})
OFIM/CNF	24.13 ± 2.91[b]	83.76 ± 1.70[a]	1.03 ± 0.12[b]
OFIM/CNF/ZnO (0.2%)	39.70 ± 4.76[a]	82.34 ± 3.29[a]	1.03 ± 0.01[b]
OFIM/CNF/ZnO (0.4%)	25.76 ± 1.63[b]	82.30 ± 3.03[a]	1.21 ± 0.32[b]
OFIM/CNF/ZnO (0.6%)	23.94 ± 0.20[b]	85.41 ± 0.33[a]	1.93 ± 0.18[a]

[a] Mean values with their corresponding ± standard deviation ($n = 3$). Numerical values with different superscript letters indicate statistically significant differences within the same column, as determined by Duncan's multiple range test ($p < 0.05$). OFIM: *Opuntia ficus-indica* mucilage; CNF: cellulose nanofiber; ZnO: zinc oxide NPs, (MC): moisture content, WS: water solubility and WVTR: water vapour transmission rate.

molecule transport. Consequently, the varying impacts of ZnO NPs on the WVTR properties of the films can be attributed to several factors, including filler concentration, polymer type, and the compatibility of the filler with the polymer matrix. Filler concentration is known to significantly affect the WVTR properties of nanocomposite films.[53] Generally, the WVTR properties of composite films decrease with the incorporation of low amounts of nanofiller, as high filler concentrations can lead to agglomerated structures, causing uneven dispersion of the nanofiller in the polymer matrix.[53,54] Overall, the higher WVTR value observed in the OFIM/CNF/ZnO (0.6%) film likely emerged from the heterogeneous dispersion of NPs in the mucilage matrix due to aggregation and possible microcracks, which may be revealed in the microscopic analysis. Further optimization of nanoparticle loading and dispersion strategies may therefore be necessary to achieve an improved balance between antimicrobial functionality and barrier performance in OFIM-based nanocomposite films.

3.4 Mechanical properties

3.4.1 Tensile strength. Mechanical properties are a critical parameter to assess the strength, flexibility, and stiffness of films, indicating the ability to maintain the structural integrity during production and transportation.[55] The tensile strength (TS) of the nanocomposite films serves as a fundamental measure of mechanical properties, reflecting the material's capacity to withstand axial loads without failure.[56] The TS of the nanocomposite films was significantly improved upon incorporating ZnO NPs, increasing from 55.95 ± 16.06 MPa to 119.28 ± 7.48 MPa. Similar findings have been reported in other studies, where the incorporation of ZnO NPs into alginate,[57] soy protein isolate,[58] and gelatin[59] films resulted in enhanced TS. An increase in the TS of the films, particularly at higher concentrations of ZnO NPs can be attributed to an even distribution and strong electrostatic and/or hydrogen bond interactions between the NPs and the polymer matrix.[60] Another possible mechanism is the filling of voids within the polymer matrix, which reduces flexibility and movement while improving crystallinity.[61] Furthermore, the results showed that a hybrid of CNF and ZnO NPs contributes to the improved mechanical properties of the nanocomposite films, rendering them suitable for packaging applications.[62]

3.4.2 Thickness. Thickness is an important parameter to determine the mechanical properties of the films. It influences stress distribution and molecular arrangement within the material, significantly affecting mechanical properties like tensile strength, elongation at break, and flexibility.[56] The obtained data for the measured thickness are presented in Table 3. The thickness of the films was significantly enhanced by incorporating ZnO ($p < 0.05$), with the highest observed maximum value found to be 0.23 ± 0.02 mm for the OFIM/CNF/ZnO (0.6%) film, significantly greater than that of the control film (0.13 ± 0.01 mm). This increase can likely be attributed to the observed surface roughness of the nanocomposite films resulting from discrete nanoparticle aggregation, as evidenced by SEM analysis. Similarly, Ortega *et al.*[63] reported comparable results, suggesting that the increased film thickness led to nanoparticle agglomeration and a higher total solid content in the film formulation containing ZnO incorporated into a banana powder matrix. Mohammadi *et al.*[64] also reported similar results when incorporating ZnO and carboxymethyl cellulose in an okra mucilage matrix.

It is worth noting here that the current study focused on tensile strength and film thickness as key indicators of mechanical performance and structural integrity in food packaging. The changes observed in tensile strength, along with supportive morphological (SEM), structural (XRD), and interaction (FTIR) analyses, provide clear evidence of improved reinforcement and film stability with the addition of CNF and ZnO. Although factors like elongation at break and elastic modulus would provide more insight into film flexibility and stiffness, these were not part of this study. Future research will

Table 3 Tensile strength and thickness of OFIM-based films incorporated with cellulose nanofiber and various concentrations of ZnO nanoparticles[a]

Film samples	TS (MPa)	Thickness (mm)
OFIM/CNF	55.95 ± 16.06[b]	0.13 ± 0.01[b]
OFIM/CNF/ZnO (0.2%)	100.61 ± 15.14[a]	0.17 ± 0.02[b]
OFIM/CNF/ZnO (0.4%)	108.35 ± 5.97[a]	0.18 ± 0.05[ab]
OFIM/CNF/ZnO (0.6%)	119.28 ± 7.48[a]	0.23 ± 0.02[a]

[a] Mean values with their corresponding ± standard deviation ($n = 3$). Numerical values with different superscript letters indicate statistically significant differences within the same column, as determined by Duncan's multiple range test ($p < 0.05$). OFIM: *Opuntia ficus-indica* mucilage; CNF: cellulose nanofiber; ZnO: zinc oxide, TS: tensile strength.

include a broader mechanical evaluation to better characterize the deformation behavior and flexibility of the films.

3.5 Light transmittance and opacity

3.5.1 Light transmittance. The assessment of light transmittance evaluates the capacity of the film to preserve the product while controlling light exposure that could cause quality degradation in packaged foods.[65] It was observed that the light transmittance capacity decreased with increasing concentrations of ZnO NPs due to greater absorption of visible light and fewer photons present in the free path.[61] At 800 nm, light transmittance decreased from 11.62 ± 1.04% in the control film to 1.60 ± 0.30% and 2.43 ± 0.46% in the OFIM/CNF/ZnO (0.4% and 0.6%) films, respectively. Across the entire wavelength range, all films containing ZnO NPs exhibited a similar pattern of reduced light transmittance, making them suitable for packaging food products prone to oxygen degradation due to UV light exposure.[66] A similar trend was observed with the incorporation of ZnO NPs into buckwheat starch films.[67]

3.5.2 Opacity. The opacity of the films was significantly influenced ($p < 0.05$) by the incorporation of ZnO as indicated in Table 4. The control film (OFIM/CNF) showed the lowest opacity (10.30 ± 0.12), which was lower than the nanocomposite films. Conversely, OFIM/CNF/ZnO (0.4%) film displayed the highest opacity (15.74 ± 0.75). Comparably, the incorporation of ZnO NPs in chitosan,[68] konjac glucomannan/chitosan,[69] and gelatin/cellulose nanofiber matrices[61] resulted in increased film opacity. Notably, a slight reduction in opacity was observed at the higher nanoparticle loading; however, it remained greater than that of the control film.

3.6 Surface morphology

Surface morphology analysis is an essential study because it shows how well the additional components, like the NPs, disperse and/or integrate within the matrix of OFIM, which consequently affects the resulting barrier, mechanical, and overall functional properties.[6] The micrograph obtained is presented in Fig. 2. The control film (OFIM/CNF) exhibited homogeneity without visible cracks, characterized by a smooth surface morphology, suggesting exceptional compatibility between CNF and the OFIM film matrix (Fig. 2a). However, incorporation of ZnO led to visible changes in the surface morphology, particularly at higher concentrations. The OFIM/CNF/ZnO (0.2%) film remained smooth without visible cracks, demonstrating an excellent nanoparticle dispersion. Similarly, the OFIM/CNF/ZnO (0.4%) film retained the smooth surface trait but displayed few cracks, while the OFIM/CNF/ZnO (0.6%) film exhibited surface roughness due to discrete aggregation and cracks embedded within the film matrix. These distinct morphological changes suggest effective integration of ZnO NPs within the mucilage matrix. Previous studies have reported comparable findings regarding the incorporation of ZnO NPs into a banana powder matrix,[6] carboxymethyl cellulose–chitosan–oleic acid film matrix,[70] basil seed mucilage–polyvinyl alcohol composites[71] and chitosan (CS)/polyvinyl alcohol (PVA)/gelatin (GE) film matrix.[72] Additionally, a study conducted by Darvish & Ajji[73] identified a smooth and homogeneous surface morphology in polyethylene film matrices infused with ZnO NPs, indicating effective interaction between the matrix and NPs, which facilitates the uniform dispersion of the NPs, particularly at lower concentrations.

Moreover, well-dispersed small white particles were observed in all film formulations. Although these particles (in the control film) visually resemble ZnO NPs, as reported in other studies,[6,71] their appearance is attributed to the presence of trace elements and starch granules found in natural biopolymers.[48] The presence of starch granules was also observed in bio-composite films incorporated with carboxymethyl cellulose, mucilage, and glycerol.[48,74] This observation was further corroborated by Energy Dispersive Spectroscopy (EDS) analysis (Fig. 3), which revealed trace elements such as potassium (K), magnesium (Mg), and phosphorus (P) in the control film (OFIM/CNF). Nevertheless, all nanocomposite films (0.2%, 0.4%, and 0.6% of ZnO) exhibited peaks for zinc and oxygen, confirming the incorporation of ZnO alongside other existing trace elements within the film matrix. This finding aligns with the research conducted by Biswas *et al.*[48] which reported bio-composite films incorporating carboxymethyl cellulose, glycerol, and ZnO NPs exhibiting rough surface morphology with uniformly dispersed ZnO NPs and a lack of agglomeration. A similar surface structure of nanocomposite films was observed with ZnO infusion, such as carboxymethyl cellulose/ZnO NPs,[75] and gelatin/ZnO NPs.[4]

Table 4 Light transmittance (%) and opacity (600 nm) of OFIM-based films incorporated with cellulose nanofiber and various concentrations of ZnO nanoparticles[a]

	Light transmittance (%)					
Film samples	400 ± SD	500 ± SD	600 ± SD	700 ± SD	800 ± SD	Opacity (600 nm)
OFIM/CNF	2.01 ± 0.21^{a}	4.45 ± 0.43^{a}	6.68 ± 0.65^{a}	9.09 ± 0.86^{a}	11.62 ± 1.04^{a}	10.30 ± 0.12^{c}
OFIM/CNF/ZnO (0.2%)	0.44 ± 0.19^{b}	1.35 ± 0.30^{b}	1.98 ± 0.41^{b}	2.55 ± 0.53^{b}	3.20 ± 0.68^{b}	13.47 ± 1.30^{b}
OFIM/CNF/ZnO (0.4%)	0.15 ± 0.08^{b}	0.79 ± 0.14^{b}	1.13 ± 0.19^{b}	1.35 ± 0.24^{b}	1.60 ± 0.30^{b}	15.74 ± 0.75^{a}
OFIM/CNF/ZnO (0.6%)	0.59 ± 0.14^{b}	1.26 ± 0.25^{b}	1.67 ± 0.31^{b}	2.05 ± 0.38^{b}	2.43 ± 0.46^{b}	10.86 ± 0.18^{c}

[a] Mean values are presented with their corresponding ± standard deviation ($n = 3$). Numerical values with different superscript letters indicate statistically significant differences within the same column, as determined by Duncan's multiple range test ($p < 0.05$). OFIM: *Opuntia ficus-indica* mucilage; CNF: cellulose nanofiber; ZnO: zinc oxide NPs.

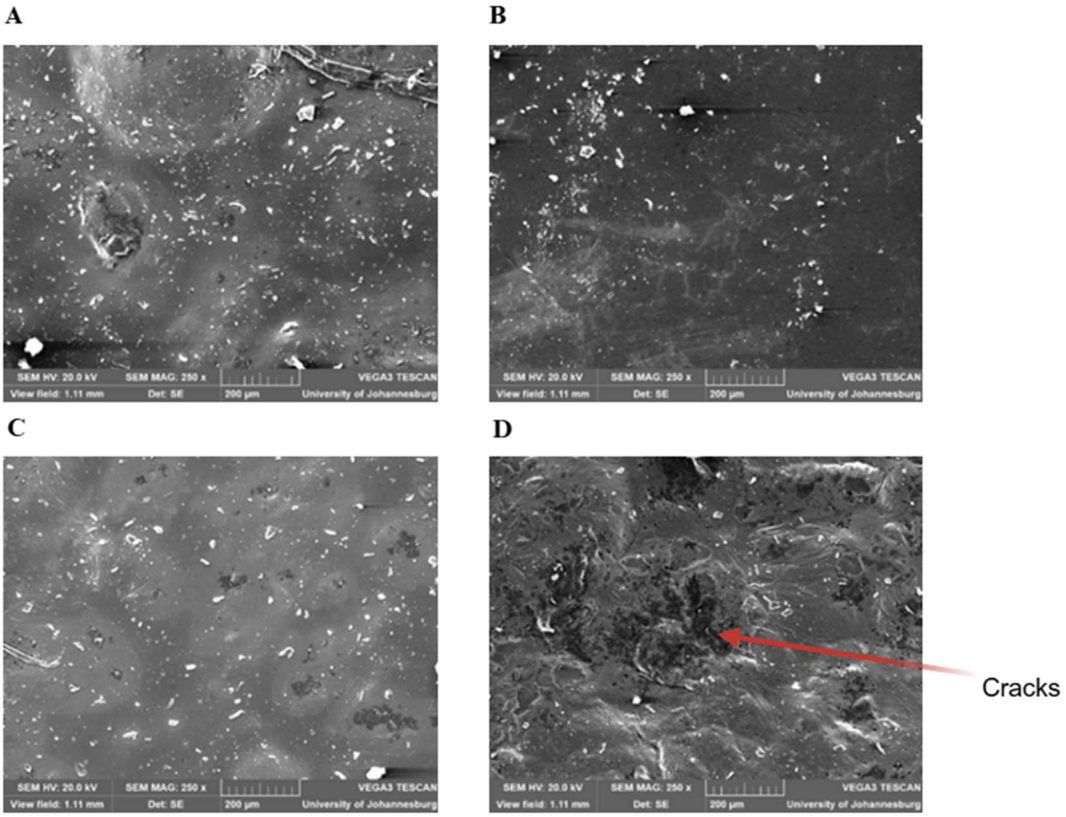

Fig. 2 Microstructural traits of OFIM-based films incorporated with different concentrations of ZnO. OFIM: *Opuntia ficus-indica* mucilage; CNF: cellulose nanofiber; ZnO: zinc oxide NPs. Notes: (A) OFIM/CNF, (B) OFIM/CNF/ZnO (0.2%), (C) OFIM/CNF/ZnO (0.4%) and (D) OFIM/CNF/ZnO (0.6%).

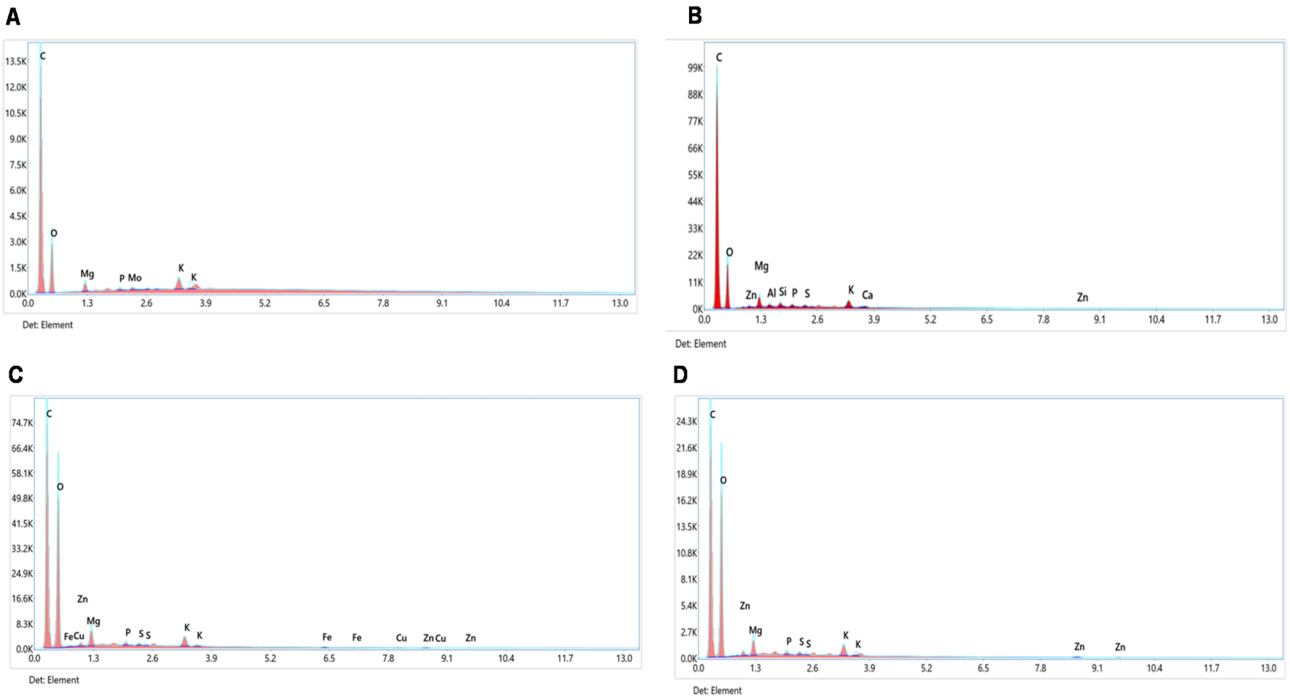

Fig. 3 Elemental analysis of OFIM-based films incorporated with different concentrations of ZnO. OFIM: *Opuntia ficus-indica* mucilage; CNF: cellulose nanofiber; ZnO: zinc oxide NPs. Notes: (A) OFIM/CNF, (B) OFIM/CNF/ZnO (0.2%), (C) OFIM/CNF/ZnO (0.4%) and (D) OFIM/CNF/ZnO (0.6%).

3.7 X-ray diffraction (XRD) patterns

XRD analysis was conducted to evaluate the crystallinity of the formulated nanocomposite films. As illustrated in Fig. 4, the control film (OFIM/CNF) and all nanocomposite films exhibited a broad diffraction band at $2\theta = 22°$, attributed to the semi-crystalline amorphous nature of biopolymers, particularly the polysaccharide mucilage, consistent with other literature reports.[8,76] Specifically, this observation aligns with previous studies using natural biopolymers such as *Plantago major* L. seed mucilage (PMSM)–polyvinyl alcohol (PVA) matrix and basil seed mucilage (a heteropolysaccharide)–polyvinyl alcohol matrix, with broad peaks around 2θ of 21.6° and 20.6°, respectively.[71,76] Although previous studies found distinct crystalline diffraction peaks linked to the hexagonal wurtzite structure of ZnO nanoparticles when added to various biopolymer matrices like carboxymethyl cellulose,[75] banana powder,[6] basil seed mucilage with polyvinyl alcohol,[71] *Plantago major* L. seed mucilage with polyvinyl alcohol,[76] and chia seed mucilage,[77] this study did not detect any clear diffraction peaks for ZnO in the nanocomposite films. Normally, ZnO shows specific peaks corresponding to the hexagonal wurtzite structure (ICDD PDF No. 36-1451); however, these peaks were not clearly defined in the XRD patterns of the OFIM-based films. The absence of discernible ZnO diffraction peaks may be attributed to the relatively low nanoparticle loading and their homogeneous dispersion within the OFIM/CNF matrix (below the XRD detection limit), thereby masking ZnO crystalline signals due to the predominantly amorphous nature of the film matrix.[78] This observation further corroborated the finding in the SEM analysis, which revealed well-dispersed nanoparticles within the film matrix characterized by a smooth surface morphology. Similar behavior has been reported in ZnO-containing biopolymer composites, where ZnO diffraction peaks become weak, attenuated, or not distinctly detectable because of low nanoparticle loading, dominant scattering from the amorphous polymer matrix, peak overlap/masking, and strong nanoparticle dispersion or interfacial interactions within the film network.[79]

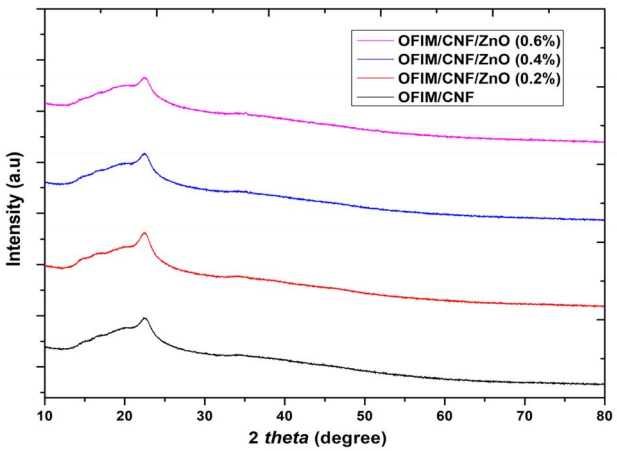

Fig. 4 X-ray diffractogram of OFIM-based films incorporated with different concentrations of ZnO. OFIM: *Opuntia ficus-indica* mucilage; CNF: cellulose nanofiber; ZnO: zinc oxide NPs.

3.8 Fourier transform infrared (FTIR) analysis

Fourier Transform Infrared (FTIR) analysis was conducted to evaluate the structural interactions among ZnO NPs, OFIM, and CNF. As depicted in Fig. 5, a similar spectral pattern was observed across all films, except for minor peaks at approximately 1746.78 and 1738.20 cm^{-1} present in the OFIM/CNF and OFIM/CNF/ZnO (0.6%) films, respectively. The spectral pattern for the OFIM/CNF/ZnO (0.4%) film was more comparable to that of the OFIM/CNF/ZnO (0.2%) film. Furthermore, upon

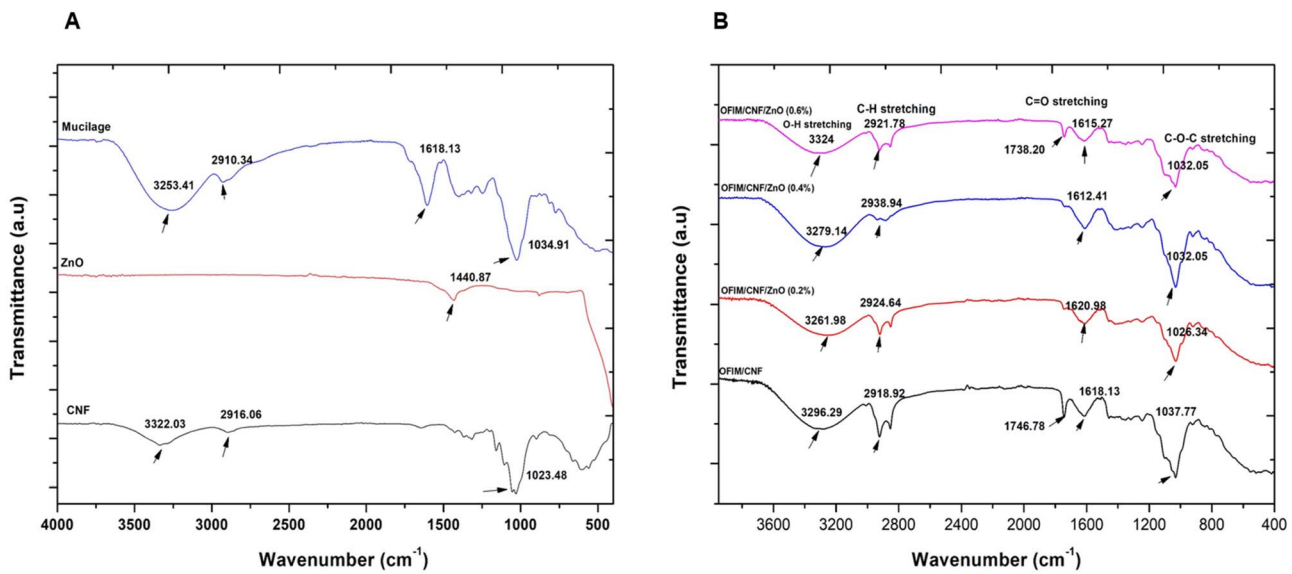

Fig. 5 The FTIR of raw materials used (A) and OFIM-based films incorporated with different concentrations of ZnO NPs (B). OFIM: *Opuntia ficus-indica* mucilage; CNF: cellulose nanofiber; ZnO: zinc oxide NPs.

incorporation of ZnO in the film matrix, a slight reduction of peak intensity was observed, particularly around 2921.78 and 2938.94 cm^{-1}. However, no peak position changes were observed, suggesting effective interaction of OFIM and ZnO NPs. In addition, characteristic absorption peaks between 3324 and 3396.20 cm^{-1} attributed to O–H stretching vibrations were found in the cellulose nanofiber and mucilage-based matrix.[80–82] Peaks around 2918.92 and 2938.94 cm^{-1} correspond to C–H stretching found in OFIM and CNF,[8] while peaks between 1612.41 and 1746.78 cm^{-1} are attributed to C=O stretching, possibly found in uronic acids and galactosyl polysaccharide residues of OFIM.[83] Other minor bands around 1026.34 and 1037.77 cm^{-1} correspond to C–O–C stretching vibrations of polysaccharide chains.[84] Comparable findings were reported by Hasheminya *et al.*,[71] Emir *et al.*,[85] and Biswas *et al.*[48]

3.9 Biological properties

3.9.1 Antioxidant properties. Evaluating the antioxidant properties of nanocomposite films is crucial for packaging fresh produce that is prone to oxidation, thus prolonging their shelf life.[5] In this study, three antioxidant assays ($ABTS^+$, DPPH, and FRAP) were used to assess the antioxidant activity and antioxidant capacity of OFIM-based films compared to the positive control (ascorbic acid). Across all assays, ascorbic acid significantly outperformed all OFIM-based films. In the $ABTS^+$ assay, no significant difference was observed among the nanocomposite films (ranging from 63 to 68.57%); however, their antioxidant potential remained higher than that of the control film (51.43%). Similarly, in the DPPH assay, the antioxidant activity of the nanocomposite films was higher than that of the control film, with the OFIM/CNF/ZnO (0.2%) film showing the highest inhibition. This pattern demonstrates that although ZnO NPs contribute to free radical scavenging, the potential can be affected by nanoparticle agglomeration or interactions with the polymer matrices, particularly at higher quantities. Moreover, FRAP results supported the antioxidant potential of the nanocomposite films, showing a concentration-dependent pattern, with reducing power ranging from 0.39 to 0.49 mM TE mg^{-1}, compared with the control film, which exhibited 0.30 mM TE mg^{-1}. These results are comparable to those reported by Leta *et al.*[6] where ZnO NPs were incorporated into a banana powder matrix, resulting in FRAP values ranging from 2.05 to 2.35 mM TE mL^{-1} DM, 58.69 to 75.60% inhibition for DPPH, and 65.19 to 76.14% for $ABTS^+$. Similarly, Hajji *et al.*[86] observed a concentration-dependent antioxidant effect in chitosan–poly(vinyl alcohol) films embedded with silver nanoparticles, with DPPH inhibition ranging from 34.96 to 57.08% and FRAP values (OD_{700} nm) ranging from 0.12 to 0.50 (Fig. 6).

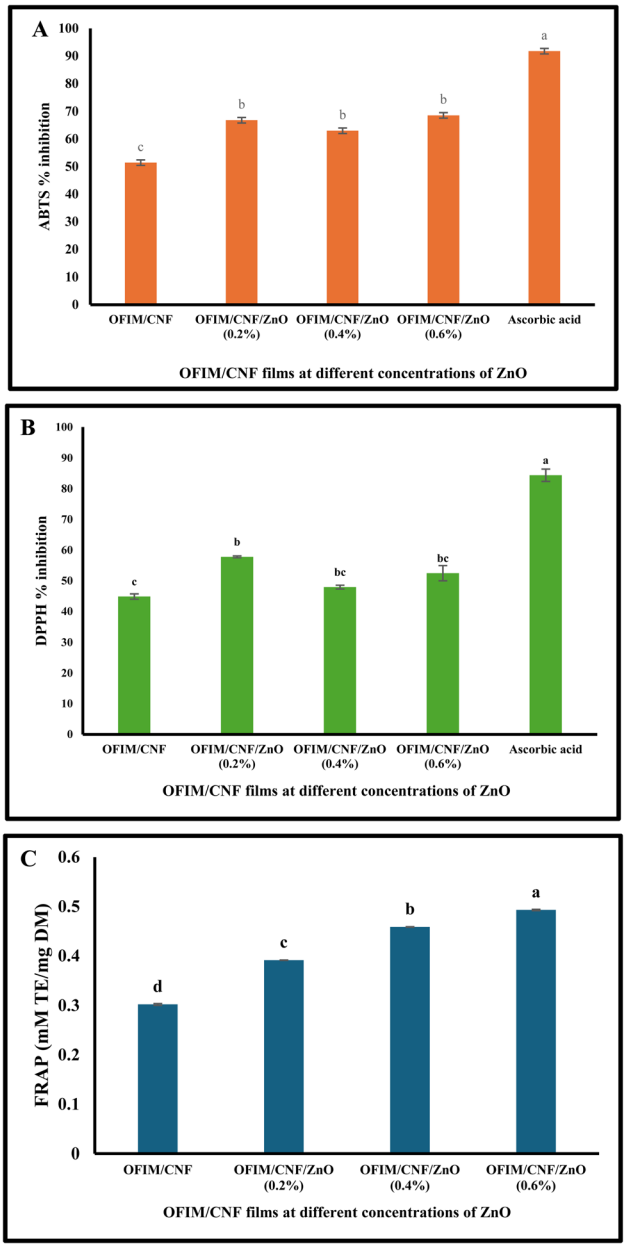

Fig. 6 Antioxidant activity of OFIM-based films incorporated with different concentrations of ZnO NPs. Notes: (A) ABTS, (B) DPPH, and (C) FRAP. OFIM: *Opuntia ficus-indica* mucilage; CNF: cellulose nanofiber; ZnO: zinc oxide NPs; ABTS – 2,2′-azino-bis(3-ethylbenzothiazoline-6-sulfonic acid), DPPH – 2,2-diphenyl-1-picrylhydrazyl, FRAP – ferric reducing antioxidant power.

3.9.2 Antimicrobial properties. Assessing antimicrobial activity is crucial for active food packaging materials to prolong the shelf life of food products by inhibiting microbial proliferation.[87] Hence, antimicrobial properties of OFIM-based films infused with various concentrations of ZnO NPs were assessed against *Staphylococcus aureus*, *Escherichia coli*, *Listeria monocytogenes,* and *Candida albicans* utilizing the agar disc diffusion method. The obtained results are presented in Table 5, and the various images depicting the zones of inhibition for each tested microbe are shown in Fig. 7. The control film (OFIM/CNF) and all nanocomposite films showed antimicrobial activity against all tested bacteria, as OFIM has also been reported to exhibit inhibitory activity against common food-borne pathogens due to its polyphenol content.[88] Previous studies have reported that OFIM has appreciably inhibited the growth of food-borne pathogens such as *Escherichia coli*, *Staphylococcus aureus*, *Pseudomonas fluorescens*, and *Salmonella typhimurium*.[88,89] For *Staphylococcus aureus*, no statistically significant difference ($p >$

Table 5 Antimicrobial properties of OFIM-based films incorporated with cellulose nanofiber and various concentrations of ZnO nanoparticles[a]

	Zone of inhibition (mm)			
Film samples	*S. aureus* ATCC 29213	*E. coli* ATCC 35218	*L. monocytogenes* ATCC 7644	*C. albicans* ATCC 14053
Neomycin	7.00 ± 0.58[b]	9.67 ± 0.33[a]	9.67 ± 0.88[b]	ND
Voriconazole	—	—	—	30.85 ± 0.44
OFIM/CNF	12.00 ± 0.33[a]	9.67 ± 0.33[a]	15.67 ± 1.00[a]	ND
OFIM/CNF/ZnO (0.2%)	11.33 ± 0.33[a]	8.33 ± 0.33[b]	15.00 ± 1.00[a]	ND
OFIM/CNF/ZnO (0.4%)	12.00 ± 1.0[a]	9.33 ± 0.33[ab]	17.33 ± 1.33[a]	ND
OFIM/CNF/ZnO (0.6%)	12.00 ± 1.15[a]	10.00 ± 0.58[a]	17.67 ± 1.76[a]	ND

[a] Mean values with their corresponding ± standard deviation ($n = 3$). Numerical values with different superscript letters indicate statistically significant differences within the same column, as determined by Duncan's multiple range test ($p < 0.05$). OFIM: *Opuntia ficus-indica* mucilage; CNF: cellulose nanofiber; ZnO: zinc oxide NPs; ND: no inhibition detected, –: not tested.

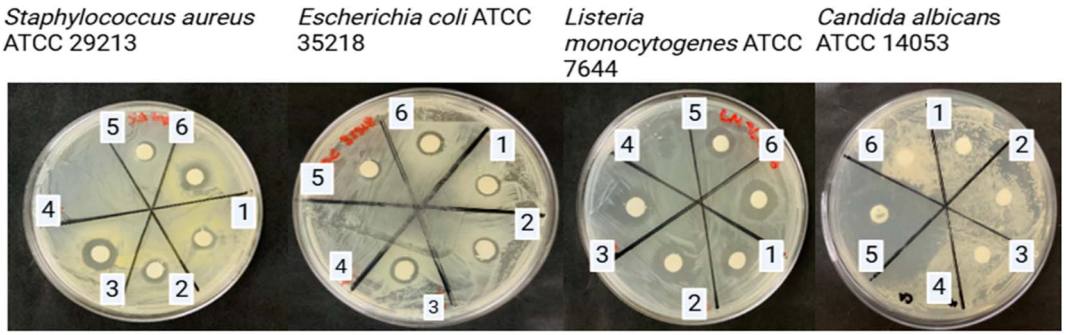

Fig. 7 Images illustrating the antimicrobial activity of OFIM-based films, shown by various zones of inhibition. Notes: (1) OFIM/CNF/ZnO (0.2%), (2) OFIM/CNF/ZnO (0.4%), (3) OFIM/CNF/ZnO (0.6%), (4) Blank, (5) neomycin/voriconazole (positive control), (6) OFIM/CNF. OFIM: *Opuntia ficus-indica* mucilage; CNF: cellulose nanofiber; ZnO: zinc oxide NPs.

0.05) was observed upon incorporation of ZnO NPs, with the zone of inhibition ranging from 11.33 to 12.00 mm. For *Escherichia coli*, a slight decrease in inhibitory activity was observed at OFIM/CNF/ZnO (0.2%) film (8.33 mm), which was significantly lower than the control film (9.67 mm); however, the inhibitory activity improved at higher concentrations, particularly at OFIM/CNF/ZnO (0.6%) (10 mm), although the difference compared to the control film was not statistically significant ($p > 0.05$). Moreover, the results showed that *Listeria monocytogenes* was the most susceptible to all film formulations, with no statistically significant differences observed between the control film and the nanocomposite films ($p > 0.05$); the zone of inhibition ranged from 15.67 to 17.67 mm. Thus, the overall pathogen susceptibility to the film formulations followed the order of *Listeria monocytogenes* (Gram-positive) > *Staphylococcus aureus* (Gram-positive) > *Escherichia coli* (Gram-negative). When compared with the positive control (neomycin), the formulated films showed comparable or stronger inhibitory effects, especially against Gram-positive bacteria at the same concentration. However, unlike the tested bacterial strains, no inhibitory activity was observed against *Candida albicans* in any of the film formulations. In their study, Sharma & Ghose[90] reported that ZnO NPs exhibit inhibitory activity against *C. albicans* through direct contact with the cell membrane and disruption of the cell wall, ultimately leading to cell death. Although antifungal effects were not observed, their strong antibacterial activity against common food-borne pathogens increases their potential to prevent food contamination[91] and makes them suitable for food packaging, while their limited antifungal activity requires the addition of additional antifungal agents.

The variation in susceptibility of bacterial strains can be attributed to the structural differences between Gram-positive and Gram-negative bacteria[92] with Gram-negative bacteria (which have a thin peptidoglycan layer) being less susceptible compared to Gram-positive bacteria (which have a multilayer peptidoglycan). These nanoparticles can damage the pathogen's cell membrane and increase permeability, leading to the accumulation of nanoparticles. This, in turn, leads to the production of reactive oxygen species, which can inhibit microbial growth or cause cell death.[31] However, the precise mechanism of action of ZnO remains vague and requires further studies. These results agree with previous findings: composite films exhibit more potent inhibitory activity against Gram-positive bacteria than against Gram-negative bacteria.[6,61,93]

It is important to note that the film showed no antifungal properties against *Candida albicans*; future studies should further assess the antifungal activity of the developed films against other major postharvest fungal pathogens involved in fresh produce spoilage, such as *Botrytis cinerea*, *Alternaria* spp., and *Penicillium* spp. Nevertheless, in this current state, the

fabricated films may still enhance food preservation through their barrier properties, including reduced moisture loss and limited oxygen transfer.

3.10 Release profiling

The release kinetics of active compounds such as antioxidants and antimicrobials are important for assessing the effectiveness of active packaging in maintaining the safety and quality of various foods during prolonged storage.[94,95] Therefore, the release behaviour of OFIM-based films incorporated with various concentrations of ZnO NPs was measured at 370 nm as shown in Fig. 8. All film formulations exhibited a biphasic release profile,[96] shown by an initial rapid release phase followed by a more gradual decline phase. The maximum loading efficacy of ZnO NPs in the nanocomposite films was quantified by dilution with dH_2O. The maximum release observed at approximately 9 h for all formulations is attributed to a diffusion-controlled burst phase, driven by the fast swelling and hydration of the hydrophilic OFIM/CNF matrix, which facilitate the release of loosely bound ZnO NPs located near or at the film surface.[97] Among the tested films, the OFIM/CNF/ZnO (0.4%) film formulation exhibited the highest release efficacy, reaching 63.14% at 9 h, followed by a gradual decline from 12 to 24 h. In contrast, the 0.2% film showed lower release levels, while the OFIM/CNF/ZnO (0.6%) film exhibited a more pronounced reduction after 12 h. This decline is likely linked to nanoparticle agglomeration and sedimentation, as observed in SEM micrographs,[98] or Zn^{2+} dissolution and subsequent re-adsorption into the polymer matrix.[99]

The controlled release behaviour can be attributed to the physicochemical characteristics of the OFIM/CNF matrix, including hydrophilicity, crystallinity, porosity, and free volume of polymer chain segments.[100] Matrices with higher porosity and chain mobility promote rapid diffusion, while denser networks restrict molecular movement and reduce release rates.[100] Similar effects have been reported in cellulose acetate films with varied porosity[101] and in hydroxypropyl methylcellulose (HPMC)-based films, which showed higher release of nisin due to lower retention capacity compared to chitosan, PLA, or caseinate matrices.[102] The balanced release profile observed in the OFIM/CNF/ZnO (0.4%) film suggests strong interfacial interactions between the polymer chains and nanoparticles, which enhance the tortuosity of the diffusion path release.[103] This concentration therefore appears optimal, providing a controlled and sustained release of active compounds suitable for prolonging shelf life. Hence, the stability of ZnO nanoparticles in the OFIM/CNF/ZnO (0.4%) film is attributed to interfacial interactions and hydrogen bonding between hydroxyl-rich CNF and ZnO surfaces, which enhance nanoparticle immobilisation, reduce early diffusion, and regulate release behaviour.[97,104] These interactions strengthen the composite structure, while molecular-level mechanisms could be further explored using Density Functional Theory (DFT) simulations in future studies.[105]

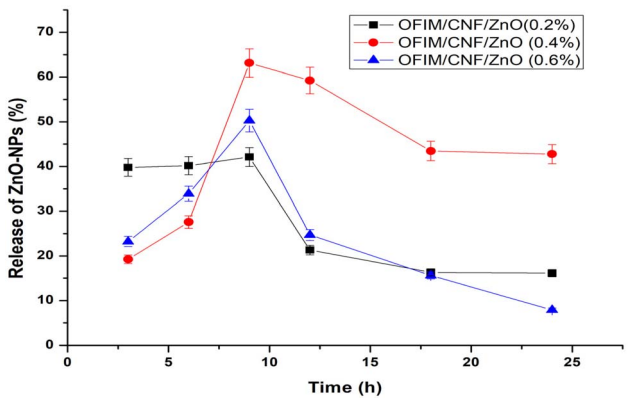

Fig. 8 Release of ZnO from OFIM-based films. OFIM: *Opuntia ficus-indica* mucilage; CNF: cellulose nanofiber; ZnO: zinc oxide NPs.

3.11 Evaluation of cherry tomato quality

3.11.1 Physiological properties

3.11.1.1 Weight loss. Weight loss serves as an indicator of tomato freshness and reflects the effectiveness of the applied coatings in delaying ripening and preserving quality.[106] As shown in Fig. 9, weight loss of the tomatoes increased progressively during the storage period across all treatments. However, the application of OFIM-based coatings significantly reduced weight loss ($p < 0.001$) compared to the uncoated control, where weight loss increased sharply from 3.90% to 21.51% between 2 d and 12 d (end of storage). In contrast, the coated tomatoes exhibited lower weight loss, increasing from 2.62%, 3.90%, and 1.88% to 16.64%, 17.44%, and 14.24% for OFIM, OFIM/CNF, and OFIM/CNF/ZnO (0.4%), respectively, over the same period. The reduction in weight loss in coated tomatoes can be attributed to the ability of the coatings to form a semipermeable barrier against solute movement, moisture, CO_2, and O_2, thereby reducing respiration and transpiration rates.[107,108] Notably, OFIM/CNF/ZnO (0.4%) outperformed both OFIM and OFIM/CNF, which may be attributed to the

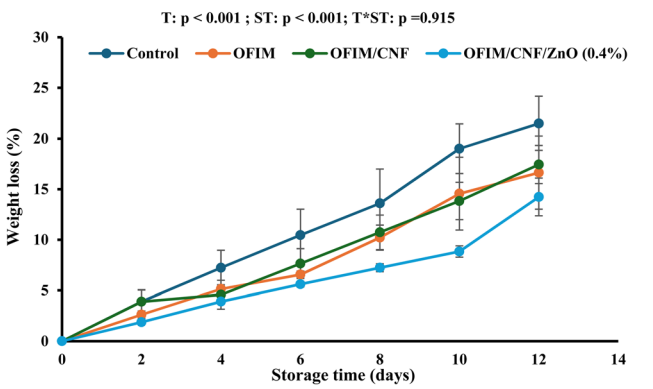

Fig. 9 The influence of *Opuntia ficus-indica* mucilage-based coatings on the weight loss of cherry tomatoes stored at ambient temperature (23 ± 2 °C). Vertical bars represent the standard errors of the mean values. T: treatment; ST: storage time; T* ST: interaction between treatment and storage time. OFIM: *Opuntia ficus-indica*. CNF: cellulose nanofiber. ZnO: zinc oxide NPs.

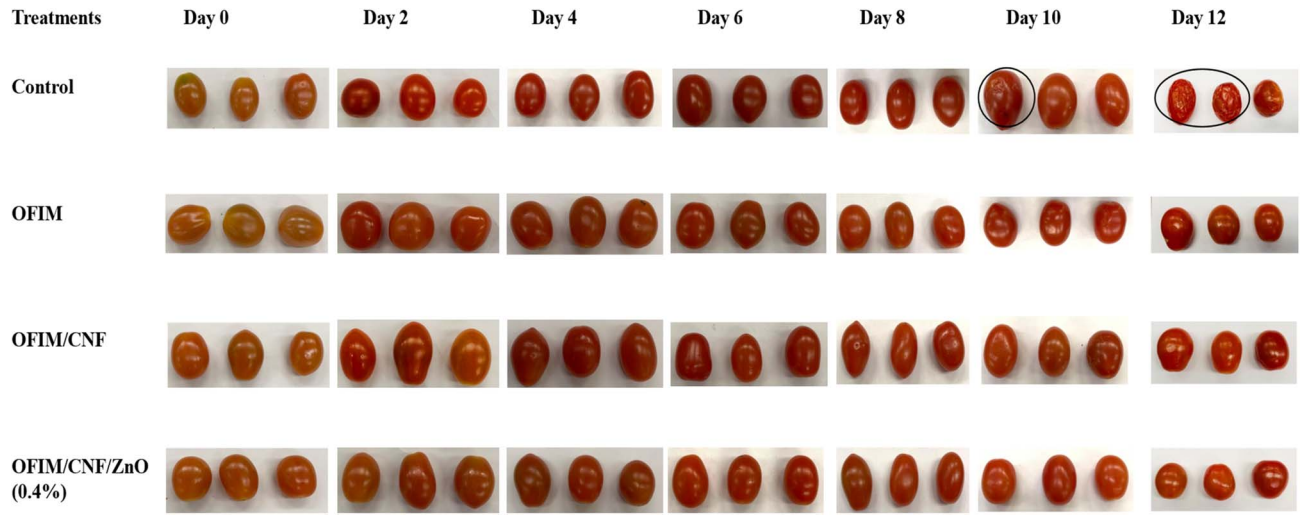

Fig. 10 Visual appearance of cherry tomatoes treated with OFIM-based coatings and of uncoated fruits at various storage periods. The circles indicate noticeable shrinkage observed in the cherry tomatoes.

antimicrobial efficacy of ZnO NPs in minimizing carbon loss associated with respiration.[109] Similar results were observed with chitosan-based coatings incorporated with ZnO NPs, which delayed the weight loss of cherry tomatoes compared to chitosan alone.[110] The visual quality changes of cherry tomatoes at various storage periods are illustrated in Fig. 10, with the control fruits showing noticeable shrinkage at the end compared to the coated fruits.

3.11.1.2 Respiration rate. Respiration rate is an important parameter to assess quality during postharvest storage, as it reflects the metabolic status of the stored commodity.[111] Throughout the storage period, the respiration rate of cherry tomatoes fluctuated significantly ($p < 0.05$). From harvest to 2 d, the respiration rate decreased, then increased up to 4 d, with OFIM/CNF showing the highest rate (17.33 mL CO_2 kg^{-1} h^{-1}), followed by the control (14.67 mL CO_2 kg^{-1} h^{-1}), OFIM (13.33 mL CO_2 kg^{-1} h^{-1}), and OFIM/CNF/ZnO (0.4%) (10.67 mL CO_2 kg^{-1} h^{-1}). By 6 d, the control, OFIM, and OFIM/CNF/ZnO (0.4%) showed comparable respiration rates, while OFIM/CNF remained higher. Despite some fluctuations, the control maintained the highest respiration rate throughout storage, peaking at 24.89 mL CO_2 kg^{-1} h^{-1}, compared to the coated tomatoes. This reflects the effectiveness of the coatings, particularly OFIM and OFIM/CNF/ZnO (0.4%), in significantly suppressing respiration. Among the coatings, OFIM/CNF/ZnO (0.4%) consistently exhibited the lowest respiration rate, likely due to its ability to efficiently mask the lenticels of the tomatoes and minimize gaseous exchange, attributed to enhanced gas barrier properties and improved membrane structure[109] compared to OFIM alone and OFIM/CNF. These findings are comparable to those reported by Hammam *et al.*,[83] who reported that alginate-based coatings infused with ZnO NPs delayed the respiration rate of 'Kiett' mangoes stored at 13 °C for 28 days. The ZnO NP-infused coatings also maintained this effect during an additional 7 days of postharvest shelf life at ambient temperature, outperforming alginate coating alone and the control (uncoated) fruits (Fig. 11).

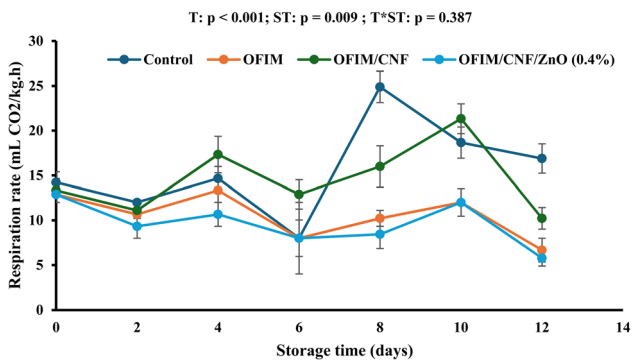

Fig. 11 The influence of *Opuntia ficus-indica* mucilage-based coatings on the respiration rate of cherry tomatoes stored at ambient temperature (23 ± 2 °C). Vertical bars represent the standard errors of the mean values. T: treatment; ST: storage time; T* ST: interaction between treatment and storage time. OFIM: *Opuntia ficus-indica*. CNF: cellulose nanofiber. ZnO: zinc oxide NPs.

3.11.1.3 Firmness. The firmness of both coated and uncoated cherry tomatoes significantly decreased ($p < 0.001$) throughout the storage period (Fig. 12). However, firmness was not significantly influenced by the interaction between storage period and treatments ($p > 0.05$), and no significant differences were observed among the treatments ($p > 0.05$). The softening of the tomatoes during storage can be attributed to cell wall degradation caused by enzymes such as pectin methylesterase, polygalacturonase, cellulase, and galactosidase.[112,113] These enzymes compromise the structural integrity of the cells, disrupt the cell membrane, and lead to the leakage of cellular contents, consequently facilitating tissue damage.[114] Furthermore, the higher respiration rate and greater weight loss observed in the uncoated tomatoes throughout storage likely accelerated tissue softening, whereas the OFIM-coated tomatoes, specifically OFIM/CNF/ZnO (0.4%) coating, exhibited

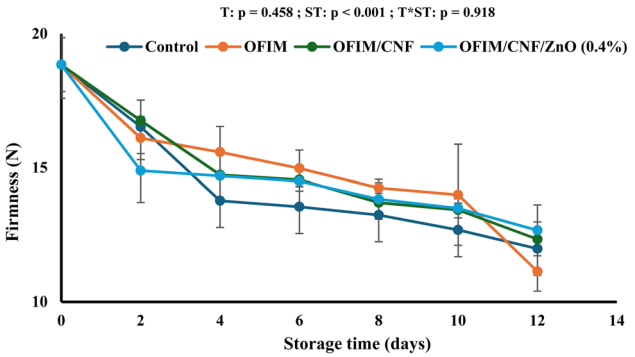

Fig. 12 The influence of *Opuntia ficus-indica* mucilage-based coatings on the firmness of cherry tomatoes stored at ambient temperature (23 ± 2 °C). Vertical bars represent the standard errors of the mean values. T: treatment; ST: storage time; T* ST: interaction between treatment and storage time. OFIM: *Opuntia ficus-indica*. CNF: cellulose nanofiber. ZnO: zinc oxide NPs.

a slight decline in firmness, attributed to reduced respiration rate.[110,115] Similarly, Leta *et al.*[42] reported a decline in pomegranate aril firmness in both banana powder-coated and uncoated groups throughout the storage period. Notably, banana powder-based coatings enriched with ZnO NPs effectively preserved aril firmness over 21 days when compared to banana-based coatings with CNF and the uncoated arils.

3.11.2 Physicochemical attributes

3.11.2.1 Color attributes. Color change is a key indicator of ripening in produce and is often used by consumers to assess product quality.[34] Significant fluctuations ($p < 0.05$) were observed in the L^* values (brightness) across the storage period, as illustrated in Fig. 13A. Tomatoes coated with OFIM/CNF/ZnO (0.4%) maintained higher L^* values until the end of storage, peaking at 28.99 on Day 4. This finding suggests a slower decline in the red coloration of the tomatoes compared to the control, OFIM, and OFIM/CNF treatments. For the a^* values (Fig. 13B), a significant increase ($p < 0.001$) was observed with prolonged storage, regardless of treatment. However, no significant differences were found among treatments ($p > 0.05$). Typically, the a^* value (redness) of cherry tomatoes increases during storage, reflecting the accumulation of lycopene, the primary pigment responsible for their characteristic red coloration.[116] Similarly, Venu *et al.*[117] also reported an increase in a^* (redness) of cherry tomatoes packaged with poly(3-hydroxybutyrate)/grapeseed oil/MgO nanocomposite packaging, attributed to its potential antioxidant effects, which efficiently inhibited lycopene degradation during postharvest storage.

3.11.2.2 Total soluble solid content and pH. The total soluble solids (TSS) of all treatments significantly increased with storage period (Fig. S2 in the SI). Although a significant interaction between the main factors was observed ($p < 0.001$), the coated cherry tomatoes exhibited a delay in TSS accumulation compared to the control group. At the end of the storage period, higher TSS was recorded for the control fruits, reaching 7.63 °Brix, followed by OFIM/CNF (7.03 °Brix), OFIM (6.93 °Brix), and OFIM/CNF/ZnO (0.4%) (5.87 °Brix), indicating variations in the ripening rate of the tomatoes. The greater TSS accumulation in uncoated tomatoes could be attributed to rapid metabolic activities such as transpiration and respiration, which promote faster ripening of fresh produce.[118] Additionally, the increase is likely due to the hydrolysis of carbohydrates, resulting in sugar production during storage.[113,118] In contrast, the maintained TSS in coated tomatoes, particularly in OFIM/CNF/ZnO (0.4%), could be attributed to the ability of the coatings to inhibit the conversion of complex polysaccharides into simple sugars.[107] Similar findings were reported by Hmmam *et al.*[119] where mangoes coated with ZnO NP-enriched alginate coatings exhibited a reduced decline in total sugar content compared to uncoated fruits during 28 days of storage at room temperature. Likewise, Buthelezi[110] also reported that uncoated cherry tomatoes exhibited higher accumulation of total and reducing sugars compared to those coated with chitosan-based coatings enriched with ZnO.

The pH of both coated and uncoated cherry tomatoes significantly increased with storage period. As shown in Fig. S3 in the SI, on 2 d, the control group exhibited a lower pH compared to the coated cherry tomatoes, and this trend persisted from 2 d to 10 d. The comparatively higher pH observed in coated tomatoes during this period could be attributed to differences in metabolic activity, particularly the utilization of organic acids as substrates for respiration during ripening.[42] At the end of the storage period (12 d), the lowest pH was recorded in cherry tomatoes coated with OFIM/CNF/ZnO (0.4%) (4.12) and OFIM (4.14). These findings suggest that the coatings, particularly OFIM/CNF/ZnO (0.4%), effectively delayed metabolic processes during storage, thereby reducing the conversion of organic acids into sugars and slowing down the senescence process.[120]

3.11.3 Phytochemical analysis

3.11.3.1 Ascorbic acid and total lycopene content. Ascorbic acid content is a crucial parameter for assessing fruit quality and antioxidative stress effects. An increased ascorbic acid content corresponds to a higher nutritional value of fruits and greater antioxidative potential.[121] The ascorbic acid (AA) content of all treatments fluctuated significantly during the storage period ($p < 0.001$). As shown in Fig. 14A, at the end of the storage period, tomatoes coated with OFIM/CNF/ZnO(0.4%) and OFIM/CNF exhibited the highest AA contents of 93.00 μg AAE mL^{-1} and 90.17 μg AAE mL^{-1}, respectively, followed by OFIM (82.45 μg AAE mL^{-1}), while the lowest AA content was observed in the control group (76.77 μg AAE mL^{-1}). The pronounced decline in AA content in control tomatoes between 8 d and 12 d could be attributed to natural ripening and senescence of the tomatoes.[122] Additionally, this decrease may result from the conversion of AA to dehydroascorbic acid by AA oxidase.[109] The availability of O_2 in respiring tomato tissues can influence AA concentration,[122] thus, the observed decline in AA content in uncoated tomatoes could be due to oxygen availability and the susceptibility of AA to enzymatic and chemical oxidation. A similar finding was reported by Dulta *et al.*[109] where orange fruits coated with an alginate–chitosan-based coating incorporated with ZnO NPs showed a greater gradual increase (33.76%), particularly on day 15, compared to uncoated fruits (12.30%).

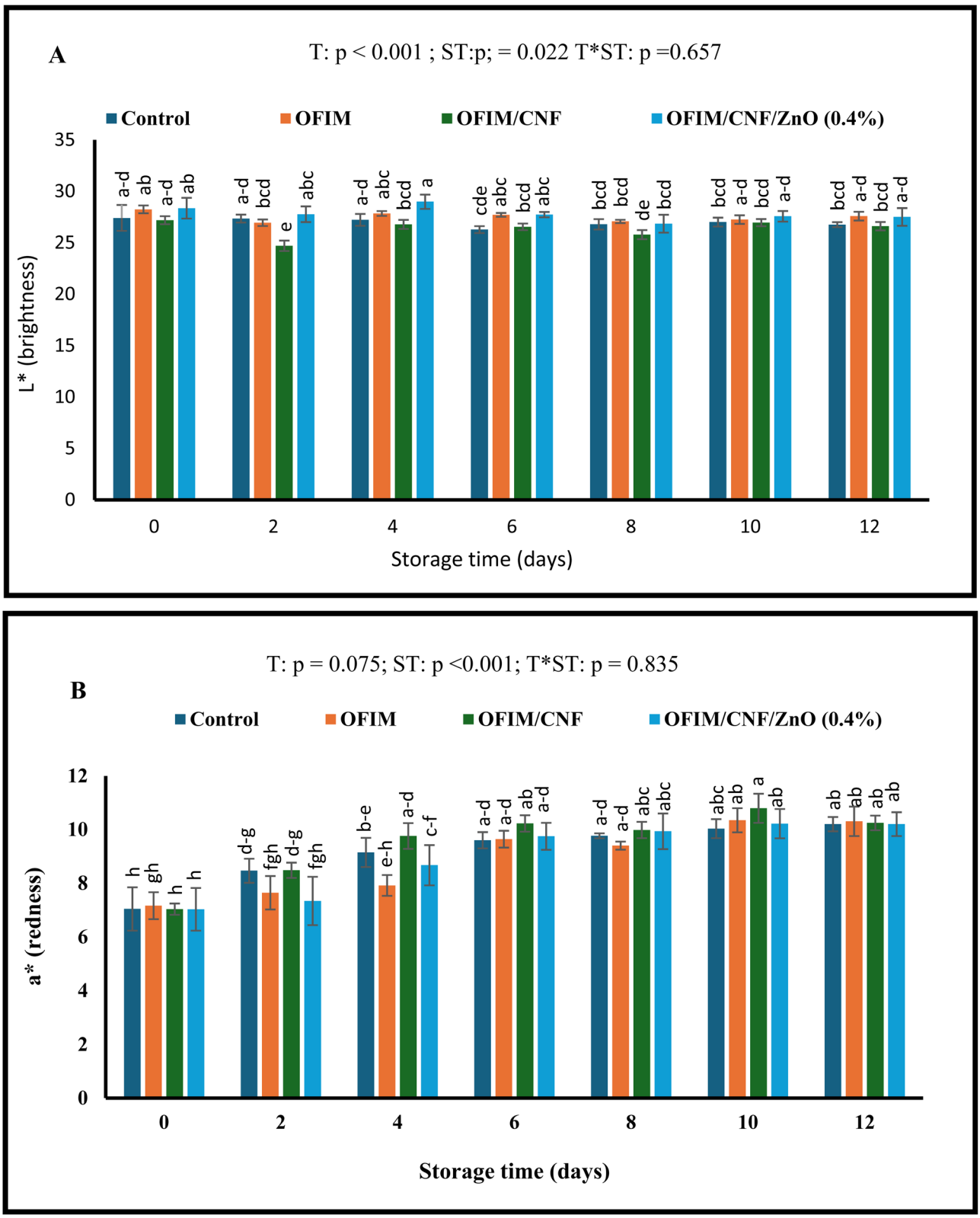

Fig. 13 The influence of *Opuntia ficus-indica* mucilage-based coatings on the lightness (A) and redness (B) of cherry tomatoes stored at ambient temperature (23 ± 2 °C). Vertical bars represent the standard errors of the mean values. T: treatment; ST: storage time; T* ST: interaction between treatment and storage time. OFIM: *Opuntia ficus-indica*. CNF: cellulose nanofiber. ZnO: zinc oxide NPs.

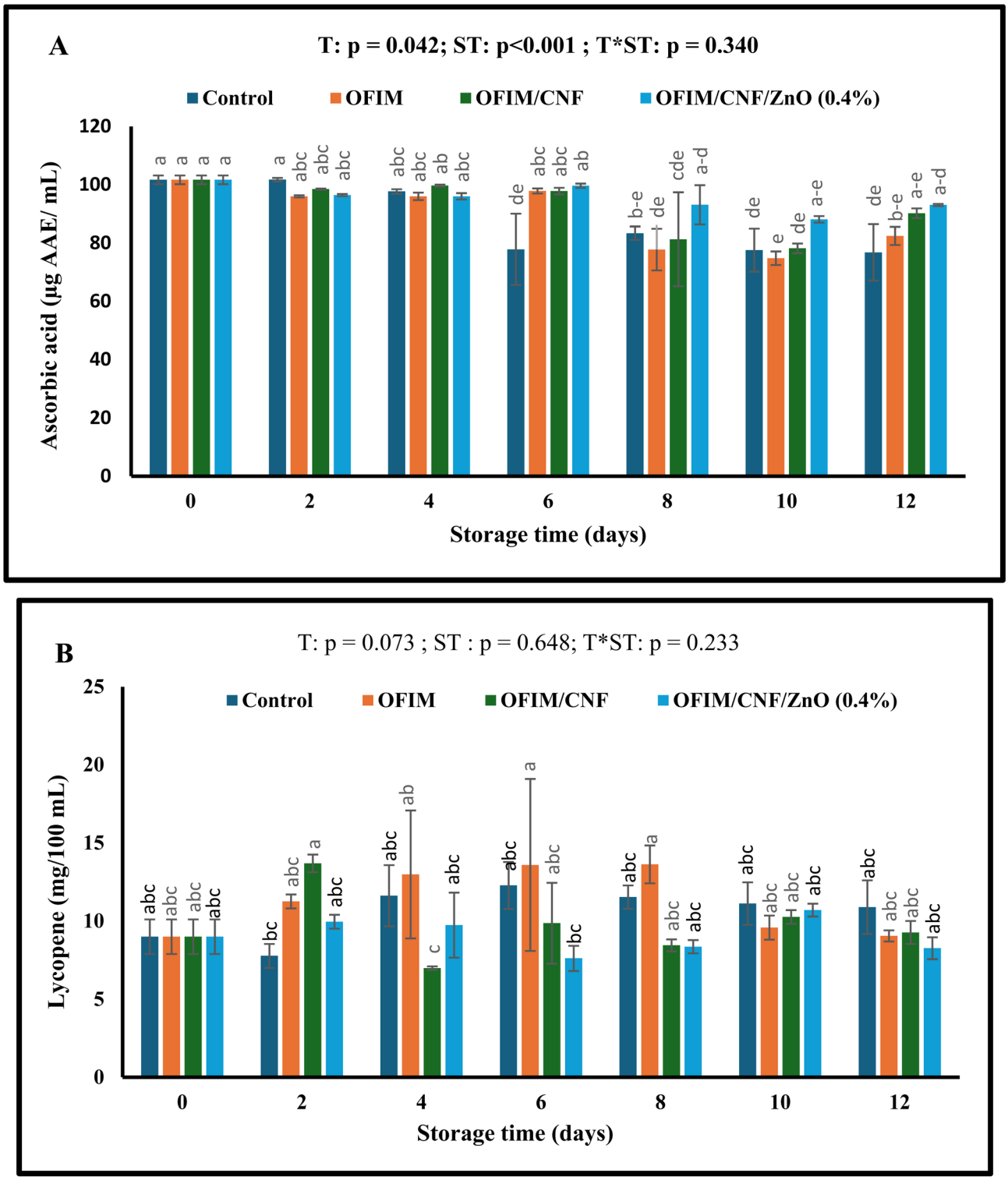

Fig. 14 The effect of *Opuntia ficus-indica* mucilage-based coatings on the ascorbic acid (A) and total lycopene content (B) of cherry tomatoes stored at ambient temperature (23 ± 2 °C). Vertical bars represent the standard errors of the mean values. T: treatment; ST: storage time; T* ST: interaction between treatment and storage time. OFIM: *Opuntia ficus-indica*. CNF: cellulose nanofiber. ZnO: zinc oxide NPs.

As shown in Fig. 14B, no significant differences were observed between treatments and storage time ($p > 0.05$). The lack of significant variation in lycopene content (responsible for the red color) regardless of treatment throughout the storage period may be attributed to the similarly non-significant changes observed in color (a^* values) between coated and uncoated tomatoes.

3.12 Discussion summary using radar analysis

The overall assessment of treatment efficacy is presented through a qualitative radar analysis, as illustrated in Fig. S4 in the SI, which incorporates all key physiological and biochemical indicators measured throughout the storage period. A normalized scoring system, ranging from 0 to 1, was developed based on the observed performance trends, with 0 indicating the weakest performance and 1 representing the strongest. In summary, the OFIM/CNF/ZnO (0.4%) formulation demonstrated superior performance, consistently maintaining high structural integrity, color, reduced weight loss, diminished respiration rates, and optimal retention of essential phytochemicals. This visualization effectively provides a concise summary of the efficacy of the OFIM/CNF/ZnO (0.4%) nanocomposites, identifying them as the optimal coating formulation for extending the shelf life of cherry tomatoes.

4 Conclusion

This investigation demonstrated that OFIM-based nanocomposite coatings can effectively maintain the postharvest quality of cherry tomatoes under ambient conditions. The incorporation of ZnO and CNF enhanced the physicochemical, mechanical, and biological characteristics of the films, validating the potential of OFI by-products as sustainable raw materials for active food packaging. ZnO NPs improved the films' light barrier and opacity properties, reduced UV-visible transmittance, and increased tensile strength. Although water vapor transmission rate slightly increased at higher concentrations due to aggregation, XRD and FTIR confirmed strong molecular interactions between ZnO NPs, CNF, and OFIM, and SEM-EDS showed uniform dispersion at moderate loadings. The ZnO-incorporated films exhibited enhanced antioxidant and antimicrobial properties, with substantial inhibition of *Staphylococcus aureus*, *Listeria monocytogenes*, and *Escherichia coli,* comparable to neomycin, underscoring their suitability for antimicrobial packaging applications. When applied as edible coatings on cherry tomatoes, the optimized OFIM/CNF/ZnO (0.4%) formulation delayed postharvest deterioration by reducing weight loss, respiration rate, and nutrient degradation while maintaining higher ascorbic acid and lycopene contents. Overall, OFIM/CNF/ZnO (0.4%) films represent a biodegradable, sustainable alternative to petroleum-based packaging. The dual valorization of *Opuntia* mucilage and peel waste for this study underscores a circular bioeconomy approach that transforms agricultural residues into high-value materials, aligning with sustainable development goals 2, 3, 9, 12, and 13.

Author contributions

Motlatsi Jane Mohlamonyane: writing – review & editing, writing – original draft, investigation, formal analysis, data curation. Jerry Oluwasegun Adeyemi: conceptualization, writing – review & editing, writing – original draft, supervision, investigation. Olaniyi Amos Fawole: conceptualization, writing – review & editing, validation, supervision, resources, project administration, funding acquisition.

Conflicts of interest

The authors declare no conflict of interest regarding the publication of this article. All funding sources supporting the research work are acknowledged within the manuscript, and there are no financial, personal, or professional relationships that could be perceived as influencing the work reported in this article. The authors confirm that the research was conducted independently and in accordance with the ethical guidelines of the RSC.

Data availability

The data supporting the findings of this study are provided in the main article and in the supplementary information (SI). Supplementary information: Table S1 – composition of OFIM-based films incorporated with cellulose nanofibers (CNFs) and various concentrations of ZnO, Fig. S1 – schematic illustration of the experimental design for coating application on cherry tomatoes. Each treatment consisted of three replicates, with five cherry tomatoes per replicate, Fig. S2 – the effect of *Opuntia ficus-indica* mucilage-based coatings on the total soluble solid content of cherry tomatoes stored at ambient temperature, Fig. S3 – the influence of *Opuntia ficus-indica* mucilage-based coatings on the pH of cherry tomatoes stored at ambient temperature, Fig. S4 – a radar plot summarizing the comparative responses of cherry tomatoes under different treatments: control (uncoated), OFIM, OFIM/CNF, and OFIM/CNF/ZnO (0.4%). A higher normalized score indicates superior preservation performance. See DOI: https://doi.org/10.1039/d6fb00067c.

Acknowledgements

The authors acknowledge the valuable support and suggestions received from the team at the Postharvest and Agroprocessing Research Centre, which have substantially improved the quality of the manuscript. This work is based on research supported by the National Research Foundation of South Africa (Ref: SPAR231013155231; CPRR23033088376), the University Research Committee at the University of Johannesburg, and the South African National Department of Agriculture (DoA) through the Agricultural Research Council of South Africa.

References

1 A. Agarwal, B. Shaida, M. Rastogi and N. B. Singh, Food Packaging Materials with Special Reference to Biopolymers-Properties and Applications, *Chem. Africa*, 2022, **6**(1), 117–144.
2 R. Farrell, Y. J. Cortese, D. M. Devine, N. Gately, M. Rueda, L. Rodriguez and R. Pezzoli, The function and properties of common food packaging materials and their suitability for reusable packaging: The transition from a linear to circular economy, *Curr. Res. Green Sustain. Chem.*, 2024, **9**, 100429.

3 S. Hussain, R. Akhter and S. S. Maktedar, *Advancements in Sustainable Food Packaging: from Eco-Friendly Materials to Innovative Technologies*, Royal Society of Chemistry, 2024, DOI: 10.1039/d4fb00084f.
4 S. Amjadi, S. Emaminia, S. Heyat Davudian, S. Pourmohammad, H. Hamishehkar and L. Roufegarinejad, Preparation and characterization of gelatin-based nanocomposite containing chitosan nanofiber and ZnO nanoparticles, *Carbohydr. Polym.*, 2019, **216**, 376–384.
5 S. Roy, H. C. Kim, P. S. Panicker, J. W. Rhim and J. Kim, Cellulose nanofiber-based nanocomposite films reinforced with zinc oxide nanorods and grapefruit seed extract, *Nanomaterials*, 2021, **11**, 877.
6 T. B. Leta, J. O. Adeyemi and O. A. Fawole, Characterization of banana powder-based film reinforced with CNF and Bio-mediated ZnO nanoparticles for potential food applications, *Mater. Res. Express*, 2024, **11**(5), 055402.
7 W. Zhang and J. W. Rhim, Titanium dioxide (TiO2) for the manufacture of multifunctional active food packaging films, *Food Packag. Shelf Life*, 2022, **31**, 100806.
8 T. Mkhari, J. O. Adeyemi and O. A. Fawole, Fabrication of active and intelligent bio-based edible films using encapsulated beetroot powders for smart packaging, *Mater. Adv.*, 2025, **6**, 1051–1066.
9 X. Yao, H. Hu, Y. Qin and J. Liu, Development of antioxidant, antimicrobial and ammonia-sensitive films based on quaternary ammonium chitosan, polyvinyl alcohol and betalains-rich cactus pears (Opuntia ficus-indica) extract, *Food Hydrocoll.*, 2020, **106**, 105896.
10 U. Urbizo-Reyes, M. F. San Martin-González, J. Garcia-Bravo and A. M. Liceaga, Development of chia seed (*Salvia hispanica*) mucilage films plasticized with polyol mixtures: Mechanical and barrier properties, *Int. J. Biol. Macromol.*, 2020, **163**, 854–864.
11 B. Hassan, S. A. S. Chatha, A. I. Hussain, K. M. Zia and N. Akhtar, Recent Advances on Polysaccharides, Lipids and Protein Based Edible Films and Coatings, *A Review., Int. J. Biol. Macromol.*, 2018, **109**, 1095–1107.
12 Y. O. Mukaila, J. O. Adeyemi and O. A. Fawole, Towards Sustainable Biopolymer Innovation: A Review of Opuntia ficus-indica Mucilage, *Processes*, 2025, **13**, 3837.
13 M. Quintero-García, E. Gutiérrez-Cortez, M. Bah, A. Rojas-Molina, M. de los A. Cornejo-Villegas, A. Del Real and I. Rojas-Molina, Comparative analysis of the chemical composition and physicochemical properties of the mucilage extracted from fresh and dehydrated opuntia ficus indica cladodes, *Foods*, 2021, **10**, 2137.
14 C. Rodrigues, C. D. de Paula, S. Lahbouki, A. Meddich, A. Outzourhit, M. Rashad, L. Pari, I. Coelhoso, A. L. Fernando and V. G. L. Souza, *Opuntia spp.: an Overview of the Bioactive Profile and Food Applications of This Versatile Crop Adapted to Arid Lands*, MDPI, 2023, DOI: 10.3390/foods12071465.
15 G. F. A. de Souza, M. M. L. Pereira, A. A. Palma e Silva, V. M. S. Capuzzo and F. Machado, Opuntia ficus-indica mucilage: A sustainable bio-additive for cementitious materials, *Constr. Build. Mater.*, 2024, **456**, 139254.
16 M. Knott and D. Diehl, Role of macromolecules on the physical properties of root and seed mucilage, *Int. J. Biol. Macromol.*, 2026, **353**, 151236.
17 A. Elshewy, F. Blando, H. Bahlol, A. El-Desouky, P. De Bellis and I. Khalifa, Egyptian Opuntia ficus-indica (OFI) Residues: Recovery and Characterization of Fresh Mucilage from Cladodes, *Horticulturae*, 2023, **9**, 736, DOI: 10.3390/horticulturae9070736.
18 M. A. D. O. S. S. Morais, K. S. Fonseca, E. K. D. Viégas, S. L. de Almeida, R. K. M. Maia, V. N. S. Silva and A. D. O. N. Simões, Mucilage of spineless cactus in the composition of an edible coating for minimally processed yam (Dioscorea spp.), *J. Food Meas. Charact.*, 2019, **13**, 2000–2008.
19 M. H. Shinga, T. Kaseke, T. M. Pfukwa and O. A. Fawole, Optimization of glycerol and cellulose nanofiber concentrations in Opuntia ficus-indica mucilage films functionalized with pomegranate peel extract for postharvest preservation of banana, *Food Packag. Shelf Life*, 2025, **47**, 101428.
20 F. J. Rodrigues, M. F. Cedran and S. Garcia, Influence of linseed mucilage incorporated into an alginate-base edible coating containing probiotic bacteria on shelf-life of fresh-cut yacon (*Smallanthus sonchifolius*), *Food Bioproc. Tech.*, 2018, **11**, 1605–1614.
21 N. Ghadiri Alamdari, S. Salmasi and H. Almasi, Tomato Seed Mucilage as a New Source of Biodegradable Film-Forming Material: Effect of Glycerol and Cellulose Nanofibers on the Characteristics of Resultant Films, *Food Bioproc. Tech.*, 2021, **14**, 2380–2400.
22 M. Mujtaba, L. Akyuz, B. Koc, M. Kaya, S. Ilk, D. Cansaran-Duman, A. S. Martinez, Y. S. Cakmak, J. Labidi and S. Boufi, Novel, multifunctional mucilage composite films incorporated with cellulose nanofibers, *Food Hydrocoll.*, 2019, **89**, 20–28.
23 T. Mkhari, T. Kaseke and O. A. Fawole, Encapsulation of betalain-rich extract from beetroot postharvest waste using a binary blend of gum Arabic and maltodextrin to promote a food circular bioeconomy, *Front. Nutr.*, 2023, **10**, DOI: 10.3389/fnut.2023.1235372.
24 H. J. Kim, S. Roy and J. W. Rhim, Effects of various types of cellulose nanofibers on the physical properties of the CNF-based films, *J. Environ. Chem. Eng.*, 2021, **9**, 106043.
25 Z. Deng, J. Jung, J. Simonsen and Y. Zhao, Cellulose nanomaterials emulsion coatings for controlling physiological activity, modifying surface morphology, and enhancing storability of postharvest bananas (Musa acuminate), *Food Chem.*, 2017, **232**, 359–368.
26 J. Jung, Z. Deng, J. Simonsen, R. M. Bastías and Y. Zhao, Development and preliminary field validation of water-resistant cellulose nanofiber based coatings with high surface adhesion and elasticity for reducing cherry rain-cracking, *Sci. Hortic.*, 2016, **200**, 161–169.
27 D. M. Nascimento, Y. L. Nunes, M. C. B. Figueirêdo, H. M. C. De Azeredo, F. A. Aouada, J. P. A. Feitosa,

M. F. Rosa and A. Dufresne, Nanocellulose nanocomposite hydrogels: technological and environmental issues, *Green Chem.*, 2018, **20**, 2428–2448.

28 K. Nagaraja and O. Tae Hwan, Green synthesis of Multifunctional Zinc oxide Nanoparticles from Cordia myxa gum; and their Catalytic Reduction of Nitrophenol, Anticancer and Antimicrobial Activity, *Int. J. Biol. Macromol.*, 2023, **253**, 126788.

29 S. Faisal, H. Jan, F. Shah, J. Hasnain, A. S. Sajjad, S. Sumaira, K. Adnan, T. A. Muhammad, R. Muhammad, J. Faheem, A. Noreen, K. Aishma and S. Suliman, Green Synthesis of Zinc Oxide (ZnO) Nanoparticles Using Aqueous Fruit Extracts of Myristica Fragrans: Their Characterizations and Biological and Environmental Applications, *ACS Omega*, 2021, **6**, 9709–9722.

30 X. Q. Zhou, Z. Hayat, D. D. Zhang, M. Y. Li, S. Hu, Q. Wu, Y. F. Cao and Y. Yuan, Zinc Oxide Nanoparticles: Synthesis, Characterization, Modification, and Applications in Food and Agriculture, *Processes*, 2023, **11**, 1193.

31 M. J. Mohlamonyane, J. O. Adeyemi and O. A. Fawole, Upcycling *opuntia ficus-indica* wastes as green mediators for functional nanomaterials: metabolomic profiling of cladode peel and mucilage residue and ZnO nanoparticle synthesis for controlling foodborne pathogens, *Mater. Res. Express*, 2025, **12**, 065402.

32 V. Ravichandran, S. Sumitha, C. Y. Ning, O. Y. Xian, U. Kiew Yu, N. Paliwal, S. A. A. Shah and M. Tripathy, Durian waste mediated green synthesis of zinc oxide nanoparticles and evaluation of their antibacterial, antioxidant, cytotoxicity and photocatalytic activity, *Green Chem. Lett. Rev.*, 2020, **13**, 102–116.

33 A. A. Tayel, N. M. Sorour, A. F. El-Baz and W. F. El-Tras, Nanometals appraisal in food preservation and food-related activities, *Food Preserv.*, 2017, 487–526.

34 M. H. Shinga and O. A. Fawole, Opuntia ficus indica mucilage coatings regulate cell wall softening enzymes and delay the ripening of banana fruit stored at retail conditions, *Int. J. Biol. Macromol.*, 2023, **245**, 125550.

35 S. Shankar, X. Teng and J.-W. Rhim, Effects of Concentration of ZnO Nanoparticles on Mechanical, Optical, Thermal, and Antimicrobial Properties of Gelatin/ZnO Nanocomposite Films, *Journal of the Korean Packaging Society*, 2014, **20**, 41–49.

36 B. Ghanbarzadeh, H. Almasi and A. A. Entezami, Physical properties of edible modified starch/carboxymethyl cellulose films, *Innov. Food Sci. Emerg. Technol.*, 2010, **11**, 697–702.

37 H. Aloui, A. R. Deshmukh, C. Khomlaem and B. S. Kim, Novel composite films based on sodium alginate and gallnut extract with enhanced antioxidant, antimicrobial, barrier and mechanical properties, *Food Hydrocoll.*, 2021, **113**, 106508.

38 Y. Li, Y. Zhou, Z. Wang, R. Cai, T. Yue and L. Cui, Preparation and characterization of chitosan–nano-zno composite films for preservation of cherry tomatoes, *Foods*, 2021, **10**, 3135.

39 S. O. Ogunyemi, Y. Abdallah, M. Zhang, H. Fouad, X. Hong, E. Ibrahim, M. M. I. Masum, A. Hossain, J. Mo and B. Li, Green synthesis of zinc oxide nanoparticles using different plant extracts and their antibacterial activity against Xanthomonas oryzae pv. oryzae, *Artif. Cells Nanomed. Biotechnol.*, 2019, **47**, 341–352.

40 S. O. Ogunyemi, Y. Abdallah, M. Zhang, H. Fouad, X. Hong, E. Ibrahim, M. M. I. Masum, A. Hossain, J. Mo and B. Li, Green synthesis of zinc oxide nanoparticles using different plant extracts and their antibacterial activity against Xanthomonas oryzae pv. oryzae, *Artif. Cells Nanomed. Biotechnol.*, 2019, **47**, 341–352.

41 S. Priyanka, S. Karthick Raja Namasivayam, F. K. John and M. Moovendhan, Starch-chitosan-Taro mucilage nanocomposite active food packaging film doped with zinc oxide nanoparticles – Fabrication, mechanical properties, anti-bacterial activity and eco toxicity assessment, *Int. J. Biol. Macromol.*, 2024, **277**, 134319.

42 T. B. Leta, J. O. Adeyemi and O. A. Fawole, Shelf-life extension of pomegranate arils using banana powder-based nanocomposite coatings functionalized with cellulose nanofiber and zinc-oxide nanoparticles, *CYTA J. Food*, 2024, **22**(1), DOI: 10.1080/19476337.2024.2405633.

43 O. A. Fawole and U. L. Opara, Effects of storage temperature and duration on physiological responses of pomegranate fruit, *Ind. Crops Prod.*, 2013, **47**, 300–309.

44 J. Tang, C. Huang, W. Liu, X. Zeng, J. Zhang, W. Liu, J. Pang and C. Wu, Preparation and characterization of a konjac glucomannan-based bio-nanocomposite film and its application in cherry tomato preservation, *Food Hydrocoll.*, 2025, **159**, 110689.

45 M. H. Shinga, O. A. Fawole and S. Pareek, Opuntia ficus-indica mucilage coating prolongs the shelf life of bananas (Musa spp.) by enhancing antioxidant activity and modulating antioxidant enzyme systems, *Food Biosci.*, 2025, **65**, 106039.

46 A. R. Davis, W. W. Fish and P. Perkins-Veazie, A rapid spectrophotometric method for analyzing lycopene content in tomato and tomato products, *Postharvest Biol. Technol.*, 2003, **28**, 425–430.

47 E. Khodaman, H. Barzegar, A. Jokar and H. Jooyandeh, Production and evaluation of Physicochemical, Mechanical and Antimicrobial Properties of Chia (*Salvia hispanica* L.) mucilage-gelatin based Edible Films Incorporated with Chitosan Nanoparticles, *J. Food Meas. Charact.*, 2022, **16**, 3547–3556.

48 A. Biswas, T. Ahmed, M. R. Rana, M. M. Hoque, M. F. Ahmed, M. Sharma, K. Sridhar, R. Ara and B. Stephen Inbaraj, Fabrication and Characterization of ZnO Nanoparticles-Based Biocomposite Films Prepared Using Carboxymethyl Cellulose, Taro Mucilage, and Black Cumin Seed Oil for Evaluation of Antioxidant and Antimicrobial Activities, *Agronomy*, 2023, **13**, 147.

49 S. K. Foghara, S. Jafarian, S. Zomorodi, A. K. asl and L. R. Nasiraei, Fabrication and characterization of an active bionanocomposite film based on basil seed

mucilage and ZnO nanoparticles, *J. Food Meas. Charact.*, 2020, **14**, 3542–3550.
50 L. I. Lim, H. L. Tan and L. P. Pui, Development and characterization of alginate-based edible film incorporated with hawthorn berry (Crataegus pinnatifida) extract, *J. Food Meas. Charact.*, 2021, **15**, 2540–2548.
51 N. Petchwattana, S. Covavisaruch, S. Wibooranawong and P. Naknaen, Antimicrobial food packaging prepared from poly(butylene succinate) and zinc oxide, *Measurement*, 2016, **93**, 442–448.
52 A. Marra, C. Silvestre, D. Duraccio and S. Cimmino, Polylactic acid/zinc oxide biocomposite films for food packaging application, *Int. J. Biol. Macromol.*, 2016, **88**, 254–262.
53 S. Shankar, L. F. Wang and J. W. Rhim, Incorporation of zinc oxide nanoparticles improved the mechanical, water vapor barrier, UV-light barrier, and antibacterial properties of PLA-based nanocomposite films, *Mater. Sci. Eng., C*, 2018, **93**, 289–298.
54 M. Mohammed, J. K. Oleiwi, A. J. afar M. Jawad, A. M. Mohammed, A. F. Osman, R. Rahman, T. Adam, B. O. Betar, S. C. B. Gopinath and O. S. Dahham, Effect of zinc oxide surface treatment concentration and nanofiller loading on the flexural properties of unsaturated polyester/kenaf nanocomposites, *Heliyon*, 2023, **9**, e20051.
55 N. Syahida, I. Fitry, A. Zuriyati and N. Hanani, Effects of palm wax on the physical, mechanical and water barrier properties of fish gelatin films for food packaging application, *Food Packag. Shelf Life*, 2020, **23**, 100437.
56 F. Hosseini, A. Gh and K. Zh, Physical and mechanical properties of nanocomposite films for sustainable packaging: An innovative biodegradable nano smart packaging approach. *Challenges in nano and micro scale science and technology*, 2024, vol. 12, pp. 12–18.
57 M. V. Aristizabal-Gil, S. Santiago-Toro, L. T. Sanchez, M. I. Pinzon, J. A. Gutierrez and C. C. Villa, ZnO and ZnO/CaO nanoparticles in alginate films. Synthesis, mechanical characterization, barrier properties and release kinetics, *LWT*, 2019, **112**, 108217.
58 J. Wu, Q. Sun, H. Huang, Y. Duan, G. Xiao and T. Le, Enhanced physico-mechanical, barrier and antifungal properties of soy protein isolate film by incorporating both plant-sourced cinnamaldehyde and facile synthesized zinc oxide nanosheets, *Colloids Surf., B*, 2019, **180**, 31–38.
59 S. Beak, H. Kim and K. Bin Song, Characterization of an Olive Flounder Bone Gelatin-Zinc Oxide Nanocomposite Film and Evaluation of Its Potential Application in Spinach Packaging, *J. Food Sci.*, 2017, **82**, 2643–2649.
60 F. Shahmohammadi Jebel and H. Almasi, Morphological, physical, antimicrobial and release properties of ZnO nanoparticles-loaded bacterial cellulose films, *Carbohydr. Polym.*, 2016, **149**, 8–19.
61 A. Ahmadi, P. Ahmadi, M. A. Sani, A. Ehsani and B. Ghanbarzadeh, Functional biocompatible nanocomposite films consisting of selenium and zinc oxide nanoparticles embedded in gelatin/cellulose nanofiber matrices, *Int. J. Biol. Macromol.*, 2021, **175**, 87–97.
62 A. A. Oun, S. Shankar and J. W. Rhim, Multifunctional nanocellulose/metal and metal oxide nanoparticle hybrid nanomaterials, *Crit. Rev. Food Sci. Nutr.*, 2020, **60**, 435–460.
63 F. Ortega, L. Giannuzzi, V. B. Arce and M. A. García, Active composite starch films containing green synthetized silver nanoparticles, *Food Hydrocoll.*, 2017, **70**, 152–162.
64 H. Mohammadi, A. Kamkar and A. Misaghi, Nanocomposite films based on CMC, okra mucilage and ZnO nanoparticles: Physico mechanical and antibacterial properties, *Carbohydr. Polym.*, 2018, **181**, 351–357.
65 M. Zam, I. Niyumsut, K. Osako and S. Rawdkuen, Fabrication and Characterization of Intelligent Multi-Layered Biopolymer Film Incorporated with pH-Sensitive Red Cabbage Extract to Indicate Fish Freshness, *Polymers*, 2022, **14**, 4914.
66 A. C. de M. Mirres, I. R. S. Vieira, L. Tessaro, B. D. da Silva, J. C. de Andrade, A. A. da Silva, N. M. F. Carvalho, A. M. F. de Sousa and C. A. Conte-Junior, Nanocomposite Films of Babassu Coconut Mesocarp and Green ZnO Nanoparticles for Application in Antimicrobial Food Packaging, *Foods*, 2024, **13**, 1895.
67 S. Kim and K. Bin Song, Antimicrobial activity of buckwheat starch films containing zinc oxide nanoparticles against Listeria monocytogenes on mushrooms, *Int. J. Food Sci. Technol.*, 2018, **53**, 1549–1557.
68 J. Liu, J. Huang, Z. Hu, G. Li, L. Hu, X. Chen and Y. Hu, Chitosan-based films with antioxidant of bamboo leaves and ZnO nanoparticles for application in active food packaging, *Int. J. Biol. Macromol.*, 2021, **189**, 363–369.
69 J. Sun, H. Jiang, H. Wu, C. Tong, J. Pang and C. Wu, Multifunctional bionanocomposite films based on konjac glucomannan/chitosan with nano-ZnO and mulberry anthocyanin extract for active food packaging, *Food Hydrocoll.*, 2020, **107**, 105942.
70 N. Noshirvani, B. Ghanbarzadeh, R. R. Mokarram, M. Hashemi and V. Coma, Preparation and characterization of active emulsified films based on chitosan-carboxymethyl cellulose containing zinc oxide nano particles, *Int. J. Biol. Macromol.*, 2017, **99**, 530–538.
71 S. M. Hasheminya, J. Dehghannya and A. Ehsani, Development of basil seed mucilage (a heteropolysaccharide) – Polyvinyl alcohol biopolymers incorporating zinc oxide nanoparticles, *Int. J. Biol. Macromol.*, 2023, **253**, 127342.
72 A. W. Ayoub, S. M. Sayed, Y. A. Hefnawy and A. M. Youssef, Innovative use of chitosan/PVA/GE/ZnO biofilms based on Sage nanoemulsion for sustainable antimicrobial packaging of chilled chicken meat parts, *J. Food Meas. Charact.*, 2025, **19**, 4961–4984.
73 M. Darvish and A. Ajji, Effect of polyethylene film thickness on the antimicrobial activity of embedded zinc oxide nanoparticles, *ACS Omega*, 2021, **6**, 26201–26209.
74 R. Wang, X. Li, L. Liu, W. Chen, J. Bai, F. Ma, X. Liu and W. Kang, Preparation and characterization of edible films

composed of Dioscorea opposita Thunb. mucilage and starch, *Polym. Test.*, 2020, **90**, 106708.
75 N. Yousefi, Y. Zahedi, A. Yousefi, G. Hosseinzadeh and M. Jekle, Development of carboxymethyl cellulose-based nanocomposite incorporated with ZnO nanoparticles synthesized by cress seed mucilage as green surfactant, *Int. J. Biol. Macromol.*, 2024, **265**, 130849.
76 S. M. Hasheminya and J. Dehghannya, Development and characterization of Plantago major L. seeds mucilage - polyvinyl alcohol nano-biocomposite films incorporating Satureja sahendica Bornm. essential oil nanoemulsion and zinc oxide nanoparticles, *Int. J. Biol. Macromol.*, 2025, **306**, 141629.
77 F. Akhavan Seiasipour Foumani, M. S. Soltani, S. Zomorodi, S. Jafarian and A. K. Asl, Effect of chia seed mucilage coating containing zinc oxide nanoparticles on shelf life of chicken fillet, *Vet. Res. Forum*, 2022, **13**, 577.
78 A. Solikhin, Y. S. Hadi, M. Y. Massijaya, S. Nikmatin, S. Suzuki, Y. Kojima and H. Kobori, Properties of Poly(Vinyl Alcohol)/Chitosan Nanocomposite Films Reinforced with Oil Palm Empty Fruit Bunch Amorphous Lignocellulose Nanofibers, *J. Polym. Environ.*, 2018, **26**, 3316–3333.
79 F. Ezzatabadipour, Z. Ghasemi and M. H. Abdolrasouli, Green fabrication of PVA based biofilms incorporated with shrimp shell derived chitosan, plasticized with PEG or Gly and reinforced by biosynthesized ZnO nanoparticles, *Sci. Rep.*, 2026, **16**, 1–20.
80 P. Ezati, H. Tajik and M. Moradi, Fabrication and characterization of alizarin colorimetric indicator based on cellulose-chitosan to monitor the freshness of minced beef, *Sens. Actuators, B*, 2019, **285**, 519–528.
81 I. Choi, J. Y. Lee, M. Lacroix and J. Han, Intelligent pH indicator film composed of agar/potato starch and anthocyanin extracts from purple sweet potato, *Food Chem.*, 2017, **218**, 122–128.
82 C. L. Luchese, N. Sperotto, J. C. Spada and I. C. Tessaro, Effect of blueberry agro-industrial waste addition to corn starch-based films for the production of a pH-indicator film, *Int. J. Biol. Macromol.*, 2017, **104**, 11–18.
83 A. Elshewy, F. Blando, H. Bahlol, A. El-Desouky, P. De Bellis and I. Khalifa, Egyptian Opuntia ficus-indica (OFI) residues: Recovery and characterization of fresh mucilage from cladodes, *Horticulturae*, 2023, **9**, 736.
84 O. García-Barradas, A. Esteban-Cortina, M. R. Mendoza-Lopez, R. I. Ortiz-Basurto, D. I. Díaz-Ramos and M. Jiménez-Fernández, Chemical modification of Opuntia ficus-indica mucilage: characterization, physicochemical, and functional properties, *Polym. Bull.*, 2023, **80**, 8783–8798.
85 O. Emir Coban, Z. Akat, P. Karatepe and G. K. Incili, In vitro bioactivity of biodegradable films based on chitosan/quince seed mucilage reinforced with ZnO-nanoparticle, *J. Food Meas. Charact.*, 2024, **18**, 5450–5461.
86 S. Hajji, R. B. S. Ben Salem, M. Hamdi, K. Jellouli, W. Ayadi, M. Nasri and S. Boufi, Nanocomposite films based on chitosan–poly(vinyl alcohol) and silver nanoparticles with high antibacterial and antioxidant activities, *Process Saf. Environ. Prot.*, 2017, **111**, 112–121.
87 W. Hu, Z. Zou, H. Li, Z. Zhang, J. Yu and Q. Tang, Fabrication of highly transparent and multifunctional polyvinyl alcohol/starch based nanocomposite films using zinc oxide nanoparticles as compatibilizers, *Int. J. Biol. Macromol.*, 2022, **204**, 284–292.
88 N. P. Mbonambi, F. Seke and O. A. Fawole, Comparative analysis of Opuntia ficus-indica mucilage and gum arabic as wall materials in anthocyanin-rich raspberry pomace microencapsulation for potential food packaging applications, *Appl. Food Res.*, 2025, **5**, 101029.
89 R. Pourmajed, M. Jabbari Amiri, P. Karami and A. Khaledi, Antimicrobial Effect of Opuntia Ficus-Indica Extract on Escherichia coli Isolated from Patients with Urinary Tract Infection, *Iran. J. Public Health*, 2021, **50**, 634.
90 R. K. Sharma and R. Ghose, Synthesis of zinc oxide nanoparticles by homogeneous precipitation method and its application in antifungal activity against Candida albicans, *Ceram. Int.*, 2015, **41**, 967–975.
91 R. Chawla, S. Sivakumar and H. Kaur, Antimicrobial edible films in food packaging: Current scenario and recent nanotechnological advancements- a review, *Carbohydr. Polym. Technol. Appl.*, 2021, **2**, 100024.
92 S. Shankar, X. Teng, G. Li and J. W. Rhim, Preparation, characterization, and antimicrobial activity of gelatin/ZnO nanocomposite films, *Food Hydrocoll.*, 2015, **45**, 264–271.
93 A. Shah, I. Hussain and G. Murtaza, Chemical synthesis and characterization of chitosan/silver nanocomposites films and their potential antibacterial activity, *Int. J. Biol. Macromol.*, 2018, **116**, 520–529.
94 L. Kuai, F. Liu, B. Sen Chiou, R. J. Avena-Bustillos, T. H. McHugh and F. Zhong, Controlled release of antioxidants from active food packaging: A review, *Food Hydrocoll.*, 2021, **120**, 106992.
95 R. Ramaswamy, J. Ahn, V. M. Balasubramaniam, L. Rodriguez Saona and A. E. Yousef, *Food Safety Engineering, Handbook of Farm, Dairy and Food Machinery Engineering*, 2nd edn, 2013, pp. 43–66.
96 Y. C. Huang, R. Y. Li, J. Y. Chen and J. K. Chen, Biphasic release of gentamicin from chitosan/fucoidan nanoparticles for pulmonary delivery, *Carbohydr. Polym.*, 2016, **138**, 114–122.
97 J. Supramaniam, D. Y. S. Low, S. K. Wong, L. T. H. Tan, B. F. Leo, B. H. Goh, D. Darji, F. R. M. Rasdi, K. G. Chan, L. H. Lee and S. Y. Tang, Facile synthesis and characterization of palm CNF-ZnO nanocomposites with antibacterial and reinforcing properties, *Int. J. Mol. Sci.*, 2021, **22**, 5781.
98 S. Ganguly and S. Chakraborty, Sedimentation of nanoparticles in nanoscale colloidal suspensions, *Phys. Lett. A*, 2011, **375**, 2394–2399.
99 Y. Han, G. Hwang, D. Kim, S. A. Bradford, B. Lee, I. Eom, P. J. Kim, S. Q. Choi and H. Kim, Transport, retention, and long-term release behavior of ZnO nanoparticle aggregates in saturated quartz sand: Role of solution pH and biofilm coating, *Water Res.*, 2016, **90**, 247–257.

100 G. Cirillo, M. Curcio, T. Spataro, N. Picci, D. Restuccia, F. Iemma and U. G. Spizzirri, Antioxidant Polymers for Food Packaging, *Food Packaging Preserv.*, 2018, 213–238.
101 S. Gemili, A. Yemenicioğlu and S. A. Altinkaya, Development of antioxidant food packaging materials with controlled release properties, *J. Food Eng.*, 2010, **96**, 325–332.
102 M. Imran, A. Klouj, A. M. Revol-Junelles and S. Desobry, Controlled release of nisin from HPMC, sodium caseinate, poly-lactic acid and chitosan for active packaging applications, *J. Food Eng.*, 2014, **143**, 178–185.
103 C. Vasile and M. Baican, Progresses in Food Packaging, Food Quality, and Safety—Controlled-Release Antioxidant and/or Antimicrobial Packaging, *Molecules*, 2021, **26**, 1263.
104 X. Li, H. Chen, L. Zhang, Z. Wang, S. Wu and J. Ma, The interface design and properties enhancement of ZnO/cellulose composites: Branching fiber network to guide the assembly of ZnO flower, *J. Colloid Interface Sci.*, 2023, **641**, 539–552.
105 E. Laudadio, E. Mohebbi, E. Pavoni, C. Minnelli, S. Sabbatini and P. Stipa, Density functional theory and molecular dynamics studies on electrical, mechanical, and thermal properties of TiO2 nanoparticles interacting with poly lactic-co-glycolic acid, *Colloids Surf., A*, 2023, **667**, 131388.
106 B. Yousuf and A. K. Srivastava, Flaxseed gum in combination with lemongrass essential oil as an effective edible coating for ready-to-eat pomegranate arils, *Int. J. Biol. Macromol.*, 2017, **104**, 1030–1038.
107 M. Akhtar, A. Akhtar, W. Nazir and N. Khalid, Formulation of Edible Coatings from Alfalfa Saponins to Enhance the Postharvest Quality of Tomatoes, *Prev. Nutr. Food Sci.*, 2023, **28**, 178.
108 M. Goswami, K. Mondal, V. Prasannavenkadesan, V. Bodana and V. Katiyar, Effect of guar gum-chitosan composites edible coating functionalized with essential oils on the postharvest shelf life of Khasi mandarin at ambient condition, *Int. J. Biol. Macromol.*, 2024, **254**, 127489.
109 K. Dulta, G. Koşarsoy Ağçeli, A. Thakur, S. Singh, P. Chauhan and P. K. Chauhan, Development of alginate-chitosan based coating enriched with ZnO nanoparticles for increasing the shelf life of orange fruits (Citrus sinensis L.), *J. Polym. Environ.*, 2022, **30**, 3293–3306.
110 N. M. D. Buthelezi, Chitosan–zinc oxide nanoparticle composite coatings preserve postharvest quality of 'Rosada' cherry tomato, *HortScience*, 2025, **60**, 613–623.
111 S. Mwelase and O. A. Fawole, Effect of Chitosan-24-Epibrassinolide Composite Coating on the Quality Attributes of Late-Harvested Pomegranate Fruit under Simulated Commercial Storage Conditions, *Plants*, 2022, **11**, 351.
112 X. Ruelas-Chacon, J. C. Contreras-Esquivel, J. Montañez, A. F. Aguilera-Carbo, M. L. Reyes-Vega, R. D. Peralta-Rodriguez and G. Sanchéz-Brambila, Guar Gum as an Edible Coating for Enhancing Shelf-Life and Improving Postharvest Quality of Roma Tomato (Solanum lycopersicum L.), *J. Food Qual.*, 2017, **2017**, 8608304.
113 A. Álvarez, J. J. Manjarres, C. Ramírez and G. Bolívar, Use of an exopolysaccharide-based edible coating and lactic acid bacteria with antifungal activity to preserve the postharvest quality of cherry tomato, *LWT*, 2021, **151**, 112225.
114 A. S. Formiga, E. M. Pereira, J. S. P. Junior, F. B. Costa and B. H. Mattiuz, Effects of edible coatings on the quality and storage of early harvested guava, *Food Chem. Adv.*, 2022, **1**, 100124.
115 T. Kathirvelu, J. R. Xavier, N. Innasimuthu and O. P. Chauhan, Exploring composite edible coatings for shelf life extension and quality preservation of tomato (Solanum lycopersicum L.), *Future Postharv. Food*, 2024, **1**, 401–413.
116 L. Li, W. Guo, L. Wang, S. Cheng and H. Cheng, Chitosan derived nano-selenium based coatings for postharvest safety of cherry tomato, *LWT*, 2025, **217**, 117441.
117 S. Venu Gopala Kumari, K. Pakshirajan and G. Pugazhenthi, Application of active and environment-friendly poly (3-hydroxybutyrate)/grapeseed oil/MgO nanocomposite packaging for prolonging the shelf-life of cherry tomatoes (Solanum lycopersicum L. var. cerasiforme), *Sustain. Chem. Pharm.*, 2024, **41**, 101681.
118 F. L. Tchouala Tazo, G. Kanmegne, A. N. Tchinda, O. J. Kenfack and E. T. Phounzong, Optimization of Edible Coating Formulation Using Response Surface Methodology for Delaying the Ripening and Preserving Tomato (Solanum lycopersicum) Fruits, *J. Food Qual.*, 2023, 7710980.
119 I. Hmmam, M. A. S. Ali and A. Abdellatif, Alginate-based zinc oxide nanoparticles coating extends storage life and maintains quality parameters of mango fruits "cv. Kiett", *Coatings*, 2023, **13**, 362.
120 S. Li, Y. Xu, Y. Bi, B. Zhang, S. Shen, T. Jiang and X. Zheng, Melatonin treatment inhibits gray mold and induces disease resistance in cherry tomato fruit during postharvest, *Postharvest Biol. Technol.*, 2019, **157**, 110962.
121 Y. Lai, W. Wang, J. Zhao, S. Tu, Y. Yin and L. Ye, Chitosan Na-montmorillonite films incorporated with citric acid for prolonging cherry tomatoes shelf life, *Food Packag. Shelf Life*, 2022, **33**, 100879.
122 M. L. Flores-López, J. M. Vieira, C. M. R. Rocha, J. M. Lagarón, M. A. Cerqueira, D. Jasso de Rodríguez and A. A. Vicente, Postharvest Quality Improvement of Tomato (Solanum lycopersicum L.) Fruit Using a Nanomultilayer Coating Containing Aloe vera, *Foods*, 2023, **13**, 83.